

Identifying Spurious Biases Early in Training through the Lens of Simplicity Bias

Yu Yang

Department of Computer Science
University of California, Los Angeles
yuyang@cs.ucla.edu

Eric Gan

Department of Computer Science
University of California, Los Angeles
egan8@ucla.edu

Gintare Karolina Dziugaite

Google DeepMind
gkdz@google.com

Baharan Mirzasoleiman

Department of Computer Science
University of California, Los Angeles
baharan@cs.ucla.edu

Abstract

Neural networks trained with (stochastic) gradient descent have an inductive bias towards learning simpler solutions. This makes them highly prone to learning simple *spurious* features that are highly correlated with a label instead of the predictive but more complex core features. In this work, we show that, interestingly, the simplicity bias of gradient descent can be leveraged to identify spurious correlations, early in training. First, we prove on a two-layer neural network, that groups of examples with high spurious correlation are separable based on the model’s output, in the initial training iterations. We further show that if spurious features have a small enough noise-to-signal ratio, the network’s output on the majority of examples in a class will be almost exclusively determined by the spurious features and will be nearly invariant to the core feature. Finally, we propose SPARE, which separates large groups with spurious correlations early in training, and utilizes importance sampling to alleviate the spurious correlation, by balancing the group sizes. We show that SPARE achieves up to 5.6% higher worst-group accuracy than state-of-the-art methods, while being up to 12x faster. We also show the applicability of SPARE to discover and mitigate spurious correlations in Restricted ImageNet.

1 Introduction

The *simplicity bias* of gradient-based training algorithms towards learning simpler solutions has been suggested as a key factor for the superior generalization performance of overparameterized neural networks [11, 12, 21, 24, 26, 32]. At the same time, it is conjectured to make neural networks vulnerable to learning *spurious* correlations frequently found in real-world datasets [28, 34]. Neural networks trained with gradient-based methods can exclusively rely on simple spurious features that exist in majority of examples in a class but are not predictive of the class in general (e.g., image background), and remain invariant to the predictive but more complex core features [32]. This results in learning non-robust solutions that do not generalize well under seemingly benign distribution shifts, or on minority groups of the original data distribution that do not contain the spurious features [32, 36].

To alleviate the effect of spurious biases in absence of group labels, existing methods partition examples in each class into a majority and a minority group. This is achieved by training the model with gradient descent and identifying the minority group as examples that are misclassified [16], have a high loss [22], or sensitive representations [6, 34], or form small representation clusters at the end of training [1, 41]. Then, a robust model is trained while upweighting [28] or upsampling [16] the

minority group, or via supervised contrastive learning [41], to alleviate the effect of the spurious feature of the majority group. This can be problematic for many real-world datasets. First, they cannot distinguish between multiple minority groups. If minority groups are imbalanced, upweighting or upsampling them to the same extent can introduce new spurious biases. Second, they tend to find *unusual* examples in the minority group. While unusual examples in curated spurious benchmark datasets are only those without the spurious feature, more realistic datasets such as ImageNet, contain outliers and noisy examples, which gather in the minority group. Upweighting or upsampling such examples harm the worst-group and total accuracy. Finally, state-of-the-art methods may increase the training time by orders of magnitude [16, 41], and become prohibitive for even medium-sized datasets.

In this work, we show that the simplicity bias of gradient descent that results in learning the spurious biases can be leveraged to provably separate majority and (multiple) minority groups, *early in training*. In particular, we analyze a two-layer fully connected neural network and identify two phases early in training. First, in the initial training iterations, the contribution of the spurious feature in a majority group to the model’s output increases linearly by the amount of spurious correlation. Afterwards, if the noise-to-signal ratio of a spurious feature is smaller than that of the core feature, the model’s output on the majority of examples in the class is almost exclusively determined by the spurious feature, and will be invariant to the core features. We show that the model’s output *provably* separates majority and (multiple) minority groups early in training. Based on the above theoretical insights, we propose a method SPARE (SePARate early and REsample), which clusters the model’s output early in training to find a number of groups, determined by the silhouette score. Then, it applies importance sampling to make the groups relatively balanced. In doing so, it effectively alleviates the effect of spurious bias without increasing the training time.

Through extensive experiments, we confirm that SPARE can achieve up to 5.6% higher worst-group accuracy compared to the state-of-the-art baselines that infer the group information on CMNIST [2], Waterbirds [28], and CelebA [17], while being up to 12x faster. Notably, SPARE achieves a comparable or even better performance compared to methods that fully or partially know the group information at training time, and is highly effective in the presence of multiple minority groups and extreme group imbalance. We also apply SPARE to discover and mitigate spurious correlations in a more realistic setting, namely in Restricted ImageNet [35]. Our results confirm the effectiveness of SPARE in finding and alleviating the spurious bias, instead of upweighting the unusual examples.

2 Related Work

Mitigating spurious bias. If group labels are known at training time, class balancing techniques [9, 7], or importance weighting [33, 5] are applied to improve the performance on smaller groups. Alternatively, one can directly minimize the worst group-level error among these groups via group robust optimization (GDRO) [28], where training is focused on examples from higher-loss groups.

If group labels are not available, existing methods aim to first infer the group information, and utilize them to robustly train the model for the second time. GEORGE [34] infers group information by clustering ERM (Expected Risk Maximization) representations and trains the second model with GDRO. LfF [22] trains two models simultaneously and upweight examples that have a high loss according to the first model while training the second model. JTT [16] and CNC [41] identify the minority group as those misclassified by the initial ERM model and upsample the minority groups. JTT trains the second robust model using ERM, and CNC applies contrastive learning to pull misclassified examples towards their class. EIIL [6] and PGI [1] rely on a reference ERM model to split training data into majority and minority groups by finding an assignment that maximizes the Invariant Risk Minimization (IRM) objective [3], i.e., the variance of the model on the two groups. Then, EIIL trains the second robust model with GDRO, and PGI minimizes the KL divergence of softmaxed logits for same-class samples across groups. CIM [35] learns input-space transformations of the data to ensure that the transformation preserves task-relevant information. Finally, if a smaller group-labeled data is available, SSA [23] applies semi-supervised learning with extra group-labeled data to infer the training group labels and then uses GDRO to train a robust model. DFR [14] first trains the model with ERM, and then retrains the last layer on the group-balanced data.

State-of-the-art methods either require extra group-labeled data [23, 14], or may fail in presence of multiple imbalanced minority groups [23, 35, 22], and noisy examples [6, 17]. Some increases the

training time by orders of magnitude [16, 23, 41]. In contrast, SPARE effectively separates the groups early in training and provide superior performance without increasing the training time.

Simplicity Bias. A recent body of work revealed the simplicity bias of (stochastic) gradient methods towards learning linear functions early in training, followed by functions of increasing complexity in later phases [11, 12, 21, 24, 26, 32]. This phenomenon is empirically observed on various fully connected (FC), convolutional, and sequential networks, such as MobileNetV2 [30], ResNet50 [10], and DenseNet121 [32]. Recently, [12] formally proved that learning dynamics of gradient descent on a two-layer FC neural network can be initially mimicked by a linear model and extended this result to multi-layer FC and convolutional networks. Simplicity bias is suggested as a reason for the good generalization performance of overparameterized neural networks. At the same time, it is *conjectured* to yield models that exclusively rely on the simplest feature and remain invariant to all predictive complex features, even when the simplest feature has less predictive power [32, 36]. However, the exact notion of the simplicity of features and the mechanism by which they are learned remain poorly understood except in certain simplistic settings [20, 32]. Here, we build on [12] and rigorously specify the required conditions and mechanism of learning spurious features by a two-layer FC network.

3 Problem Formulation

Let $\mathcal{D} = \{(\mathbf{x}_i, y_i)\}_{i=1}^n \subset \mathbb{R}^d \times \mathbb{R}$ be n training data with features $\mathbf{x}_i \in \mathbb{R}^d$, and labels $y_i \in \mathcal{C} = \{1, -1\}$.

Features & Groups. We assume every class $c \in \mathcal{C}$ has a *core* feature \mathbf{v}_c , which is the invariant feature of the class that appears in both training and test set. Besides, there is a set of *spurious* features $\mathbf{v}_s \in \mathcal{A}$ that are shared between classes but may not be present at test time. For example, in the CMNIST dataset containing images of colored hand-written digits, the digit is the core feature, and its color is the spurious feature. Assuming w.l.o.g. that all $\mathbf{v}_c, \mathbf{v}_s \in \mathbb{R}^d$ are orthogonal vectors, the feature vector of every example \mathbf{x}_i in class c can be written as $\mathbf{x}_i = \mathbf{v}_c + \mathbf{v}_s + \boldsymbol{\xi}_i$, where $\mathbf{v}_s \in \mathcal{A}$, and each $\boldsymbol{\xi}_i$ is a noise vector drawn i.i.d. from $\mathcal{N}(\mathbf{0}, \Sigma_\xi)$. We assume the noise along each feature is independent, and denoted by σ_c^2, σ_s^2 variance of the noise in the directions of $\mathbf{v}_c, \mathbf{v}_s$, respectively. Training examples can be partitioned into groups $g_{c,s}$ based on the combinations of their core and spurious features $(\mathbf{v}_c, \mathbf{v}_s)$. If a group $g_{c,s}$ contains the majority of examples in class c , it is called a majority group. A class may contain multiple minority groups, corresponding to different spurious features.

Neural Network & Training. We consider a two-layer FC neural network with m hidden neurons:

$$f(\mathbf{x}; \mathbf{W}, \mathbf{z}) = \frac{1}{\sqrt{m}} \sum_{r=1}^m z_r \phi(\mathbf{w}_r^T \mathbf{x} / \sqrt{d}) = \frac{1}{\sqrt{m}} \mathbf{z}^T \phi(\mathbf{W} \mathbf{x} / \sqrt{d}), \quad (1)$$

where $\mathbf{x} \in \mathbb{R}^d$ is the input, $\mathbf{W} = [\mathbf{w}_1, \dots, \mathbf{w}_m]^T \in \mathbb{R}^{m \times d}$ is the weight matrix in the first layer, and $\mathbf{z} = [\mathbf{z}_1, \dots, \mathbf{z}_m]^T \in \mathbb{R}^m$ is the weight vector in the second layer. Here $\phi: \mathbb{R} \rightarrow \mathbb{R}$ is a smooth or piece-wise linear activation function (including ReLU, Leaky ReLU, Erf, Tanh, Sigmoid, Softplus, etc.) that acts entry-wise on vectors or matrices. We consider the following ℓ_2 training loss:

$$\mathcal{L}(\mathbf{W}, \mathbf{z}) = \frac{1}{2n} \sum_{i=1}^n (f(\mathbf{x}_i; \mathbf{W}, \mathbf{z}) - y_i)^2. \quad (2)$$

We train the network by applying gradient descent on the loss (2) starting from random initialization¹:

$$\mathbf{W}_{t+1} = \mathbf{W}_t - \eta \nabla_{\mathbf{W}} \mathcal{L}(\mathbf{W}_t, \mathbf{z}_t), \quad \mathbf{z}_{t+1} = \mathbf{z}_t - \eta \nabla_{\mathbf{z}} \mathcal{L}(\mathbf{W}_t, \mathbf{z}_t), \quad (3)$$

Worst-group error. We quantify the performance of the model based on its highest test error across groups $\mathcal{G} = \{g_{c,s}\}_{c,s}$ in all classes. Formally, *worst-group* test error is defined as:

$$\text{Err}_{wg} = \max_{g \in \mathcal{G}} \mathbb{E}_{(\mathbf{x}_i, y_i) \in g} [y_i \neq y_f(\mathbf{x}_i; \mathbf{W}, \mathbf{z})], \quad (4)$$

where $y_f(\mathbf{x}_i; \mathbf{W}, \mathbf{z})$ is the label predicted by the model. In other words, Err_{wg} measures the highest fraction of examples that are incorrectly classified across all groups.

While for simplicity, we consider binary classification with ℓ_2 loss, our analysis generalizes to multi-class classification with CE loss, and other model architectures, as we also confirm experimentally.

¹Detailed assumptions on the activations, and initialization can be found in Appendix A.2

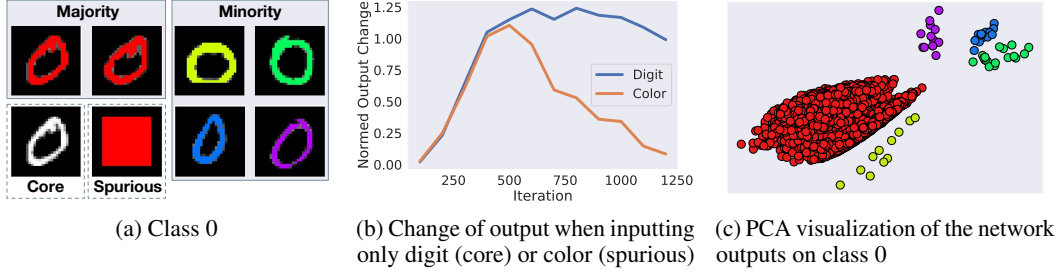


Figure 1: Training LeNet-5 on Colored MNIST containing colored handwritten digits. (a) Each digit is a class; the majority of digits in a class have a particular color, and the remaining digits are in 4 other colors. (b) The network output is almost exclusively indicated by the color of the majority group, early in training. (c) Majority and minority groups are separable based on the network output.

4 Investigating How Spurious Features are Learned by Neural Networks

We start by investigating how spurious features are learned during training a two-layer fully-connected neural network. Our analysis reveals two phases in early-time learning. First, in the initial training iterations, the contribution of a spurious feature to the network output increases linearly with the amount of the spurious correlation. Interestingly, if the majority group is sufficiently large, majority and minority groups are separable at this phase by the network output. Second, if the noise-to-signal ratio of the spurious feature of the majority group is smaller than that of the core feature, the network’s output on the majority of examples in the class will be almost exclusively determined by the spurious feature and will remain mostly invariant to the core feature. Next, we will discuss the two phases in detail.

4.1 Spurious Features are Learned in the Initial Training Iterations

We start by analyzing the effect of spurious features on the learning dynamics of a two-layer FC neural network trained with gradient descent in the initial training iterations. The following theorem shows that if a majority group is sufficiently large, the contribution of the spurious feature of the majority group to the model’s output is magnified by the network at every step early in training.

Theorem 4.1. *Let $\alpha \in (0, \frac{1}{4})$ be a fixed constant. Suppose the number of training samples n and the network width m satisfy $n \gtrsim d^{1+\alpha}$ and $m \gtrsim d^{1+\alpha}$. Let n_c be the number of examples in class c , and $n_{c,s} = |g_{c,s}|$ be the size of group $g_{c,s}$ with label c and spurious feature $\mathbf{v}_s \in \mathcal{A}$. Then, under the setting of Sec. 3 there exist a constant $\nu_1 > 0$, such that with high probability, for all $0 \leq t \leq \nu_1 \cdot \sqrt{\frac{d^{1-\alpha}}{\eta}}$, the contribution of the core and spurious features to the network output can be quantified as follows:*

$$f(\mathbf{v}_c; \mathbf{W}_t, \mathbf{z}_t) = \sqrt{\frac{2}{d}} \eta \zeta c \|\mathbf{v}_c\|^2 t \left(\frac{n_c}{n} \pm \mathcal{O}(d^{-\Omega(\alpha)}) \right), \quad (5)$$

$$f(\mathbf{v}_s; \mathbf{W}_t, \mathbf{z}_t) = \sqrt{\frac{2}{d}} \eta \zeta c \|\mathbf{v}_s\|^2 t \left(\frac{n_{c,s} - n_{c',s}}{n} \pm \mathcal{O}(d^{-\Omega(\alpha)}) \right), \quad (6)$$

where $c' = \mathcal{C} \setminus c$, and ζ is the expected gradient of activation functions at random initialization.

The proof can be found in Appendix B.2. Note that the width requirement in Theorem 4.1 is very mild as it only requires to be larger than $d^{1+\alpha}$ for some small constant α , but can be much smaller than the number of samples. The proof of Theorem 4.1 builds on the bound on the difference between training dynamics of a two-layer fully-connected neural network trained with gradient descent and that of a linear model [12] early in training, with a modest generalization that this bound holds for isolated core and spurious features, as we justify in Appendix A.1. At a high level, as the model is nearly linear in the initial $\nu_1 \cdot \frac{d \log d}{\eta}$ iterations, the contribution of the spurious feature \mathbf{v}_s to the network output grows almost linearly with $(n_{c,s} - n_{c',s}) \|\mathbf{v}_s\|^2$, at every iteration in the initial phase of training. Note that $n_{c,s} - n_{c',s}$ is the correlation between the spurious feature and the label c . When $n_{c,s} \gg n_{c',s}$, the spurious feature exists almost exclusively in the majority group of class c , and thus has a high correlation only with class c . In this case, if the magnitude of the spurious

feature is significant, the contribution of the spurious feature to the model's output grows very rapidly, early in training. In particular, if $(n_{c,s} - n_{c',s})\|\mathbf{v}_s\|^2 \gg n_c\|\mathbf{v}_c\|^2$, the model's output is increasingly determined by the spurious feature, but not the core feature.

Remember from Sec. 3 that every example consists of a core and a spurious feature. As the effect of spurious features of the majority groups is amplified in the network output, the model's output will differ for examples in the majority and minority groups. The following corollary shows that the majority and minority groups are separable based on the network's output early in training. Notably, multiple minority groups with spurious features contained in majority groups of other classes are also separable.

Corollary 4.2 (Separability of majority and minority groups). *Suppose that for all classes, a majority group has at least K examples and a minority group has at most k examples. Then, under the assumptions of Theorem 4.1, examples in the majority and minority groups are separable based on the model's output, early in training. That is, for all $0 \leq t \leq \nu_1 \cdot \sqrt{\frac{d^{1-\alpha}}{\eta}}$, with high probability, the following holds for at least $1 - \mathcal{O}(d^{-\Omega(\alpha)})$ fraction of the training examples \mathbf{x}_i in group $g_{c,s}$:*

If $g_{c,s}$ is in a majority group in class $c = 1$:

$$f(\mathbf{x}_i; \mathbf{W}_t, \mathbf{z}_t) \geq \frac{2\eta\zeta^2 t}{d} \left(\frac{\|\mathbf{v}_s\|^2(K-k)}{n} + \xi \pm \mathcal{O}(d^{-\Omega(\alpha)}) \right) + \rho(t, \phi, \Sigma), \quad (7)$$

If $g_{c,s}$ is in a minority group in class $c = 1$, but $g_{c',s}$ is a majority group in class $c' = -1$:

$$f(\mathbf{x}_i; \mathbf{W}_t, \mathbf{z}_t) \leq \frac{2\eta\zeta^2 t}{d} \left(-\frac{\|\mathbf{v}_s\|^2(K-k)}{n} + \xi \pm \mathcal{O}(d^{-\Omega(\alpha)}) \right) + \rho(t, \phi, \Sigma), \quad (8)$$

where ρ is constant for all examples in the same class, $\xi \sim \mathcal{N}(0, \kappa)$ with $\kappa = \frac{1}{n}(\sum_c n_c^2 \sigma_c^2 \|\mathbf{v}_c\|^2)^{1/2} + \frac{1}{n}(\sum_s (n_{c,s} - n_{c',s})^2 \sigma_s^2 \|\mathbf{v}_s\|^2)^{1/2}$ is the total effect of noise on the model.

Analogous statements holds for the class $c = -1$ by changing the sign and direction of the inequality.

The proof can be found in Appendix B.2. Corollary 4.2 shows that when the majority group is considerably larger than the minority groups ($K \gg k$), the prediction of examples in the majority group move toward their label considerably faster, due to the contribution of the spurious feature. Hence, majority and minority groups can be separated from each other, early in training. Importantly, multiple minority groups can be also separated from each other, if their spurious feature exists in majority groups of other classes. Note that $K > k + |\xi|$ is the minimum requirement for the separation to happen. Separation is more significant when $K \gg k$ and when $\|\mathbf{v}_s\|$ is significant.

4.2 Network Exclusively Relies on Simple Spurious Features on Majority of Examples

Next, we analyze the second phase in early-time learning of a two-layer neural network. In particular, we show that if the noise-to-signal ratio of the spurious feature of the majority group of class c , i.e., $R_s = \sigma_s/\|\mathbf{v}_s\|$ is smaller than that of the core feature $R_c = \sigma_c/\|\mathbf{v}_c\|$, then the neural network's output is almost exclusively determined by the spurious feature and remain invariant to the core feature at $T = \nu_2 \cdot \frac{d \log d}{\eta}$, even though the core feature is more predictive of the class.

Theorem 4.3. *Under the assumptions of Theorem 4.1, if the classes are balanced, and the total size of the minority groups in class c is small, i.e., $\mathcal{O}(n^{1-\gamma})$ for some $\gamma > 0$, then there exists a constant $\nu_2 > 0$ such that at $T = \nu_2 \cdot \frac{d \log d}{\eta}$, for an example \mathbf{x}_i in a majority group $g_{c,s}$, the contribution of the core feature to the model's output is at most:*

$$|f(\mathbf{v}_c; \mathbf{W}_T, \mathbf{z}_T)| \leq \sqrt{d} \frac{R_s}{\zeta R_c} + \mathcal{O}(n^{-\gamma} \sqrt{d}) + \mathcal{O}(d^{-\Omega(\alpha)}). \quad (9)$$

In particular if $\min\{R_c, 1\} \gg R_s$, then the model's output is mostly indicated by the spurious feature instead of the core feature:

$$|f(\mathbf{v}_s; \mathbf{W}_T, \mathbf{z}_T)| \geq \frac{\sqrt{d}}{2\zeta} \gg |f(\mathbf{v}_c; \mathbf{W}_T, \mathbf{z}_T)|. \quad (10)$$

The proof can be found in Appendix B.3. The proof of Theorem 4.3 shows that at $T = \nu_2 \cdot \frac{d \log d}{\eta}$ where the linear model that closely mimics early-time learning dynamics of a two-layer FC neural

network converges to its optimum parameters, the network has fully learned the spurious feature of the majority groups. At the same time, the contribution of the core feature to the network’s output is at most proportional to R_s/R_c . Hence, if $R_s \ll R_c$, the core feature does not considerably contribute to the output of the neural network at T . That is, the network almost exclusively relies on the spurious feature of the majority group instead of the core feature which is more predictive of the class.

We note that our results in Theorem 4.1, Corollary 4.2, and Theorem 4.3 generalize to more than two classes and hold if the classes are imbalanced, as we will confirm by our experiments. Similar results can be shown for multi-layer fully connected and convolutional networks, following [12].

In Figure 1 illustrates, we empirically illustrate the above results during early-time training of LeNet-5 [15] on the Colored MNIST [2] dataset containing colored handwritten digits. Here, each digit is a class. The majority of digits in each class has a particular color, and the remaining digits are in four other colors. Figure 1b shows that the prediction of the network on the majority group is almost exclusively indicated by the color of the majority group, confirming Theorem 4.3. Figure 1c shows that the majority and minority groups are separable based on the network output, confirming Corollary 4.2.

Finally, note that by only learning the spurious feature, the neural network can shrink the training loss on the majority of examples in class c to nearly zero and correctly classify them. Hence, the contribution of the spurious feature of the majority group of class c to the model’s output is retained throughout the training. On the other hand, if minority groups are small, higher complexity functions that appear later in training overfit the minority groups, as observed by [29]. This results in a small training error but a poor worst-group generalization performance on the minorities.

5 Eliminating Spurious Bias Early in Training

Next, we rely on our theoretical insights from Sec. 4 to mitigate spurious correlations while training neural networks. To do so, we first leverage the model’s output to separate majority and minority groups. Then, we apply importance sampling to amplify the effect of core features over the spurious features, by making the groups relatively balanced.

Stage 1: Separating the Groups Early in Training. Corollary 4.2 shows that majority and minority groups are separable based on the network’s output. To identify the majority and minority groups, we cluster examples V_c in every class $c \in \mathcal{C}$ based on the output of the network, during the first few epochs. We determine the number of clusters via silhouette analysis [27]. In doing so, we can separate majority and minority groups in each class. Any clustering algorithm such as k -means or k -median clustering can be applied to separate the groups. While k -means easily scales to medium-sized datasets, k -median is more suitable for very large datasets, as it can be formulated as a submodular maximization problem [39] for which fast and scalable distributed [18, 19] and streaming [4] algorithms are available. We note that following Corollary 4.2 we cluster the entire network output and not only the class confidence, which yields superior results.

Stage 2: Making the Groups More Balanced via Importance Sampling. To alleviate the spurious correlations and enable effective learning of the core features, we employ an importance sampling method on examples in each class to upsample examples in the smaller clusters and downsample examples in the larger clusters. To do so, we assign every example $i \in V_{c,j}$ a weight given by the size of the cluster it belongs to, i.e., $w_i = 1/|V_{c,j}|$. Then we sample examples in every mini-batch with probabilities equal to $p_i = w_i^\lambda / \sum_i w_i^\lambda$, where λ can be determined based on the average silhouette score of clusters in each class. A higher average silhouette score indicates that clusters are more separated. In this case, groups can be accurately identified and we can balance the groups using

Algorithm 1 SePARate early and REsample (SPARE)

Input: Network $f(\cdot, \mathbf{W})$, data $\mathcal{D} = \{(\mathbf{x}_i, y_i)\}_{i=1}^n$, loss function \mathcal{L} , iteration numbers T_N, T_{init} .

Output: Model f trained without bias

Stage 1: Early Bias Identification

for $t = 0, \dots, T_{init}$ do

$\mathbf{W}_{t+1} \leftarrow \mathbf{W}_t - \eta \nabla \mathcal{L}(\mathbf{W}_t; \mathcal{D})$

end for

for every class $c \in \mathcal{C}$ with examples V_c do

 Identify λ , # of clusters k via Silhouette analysis

 Cluster V_c into $\{V_{c,j}\}_{j=1}^k$ based on $f(\mathbf{x}_i; \mathbf{W}_t)$

 Weight every $\mathbf{x}_i \in V_{c,j}$ by $w_i = 1/|V_{c,j}|$,
 $p_i = w_i^\lambda / \sum_i w_i^\lambda$

end for

Stage 2: Learning without Bias

for $t = 0, \dots, T_N$ do

 Sample a mini-batch $\mathcal{M}_t = \{(\mathbf{x}_i, y_i)\}_i$ with probabilities p_i

$\mathbf{W}_{t+1} = \mathbf{W}_t - \eta \nabla \mathcal{L}(\mathbf{W}_t; \mathcal{M}_t)$

end for

Table 1: Worst-group and average accuracy (%) of training with SPARE vs. state-of-the-art algorithms, on datasets with spurious correlations. CB, GB indicate balancing classes and groups, respectively. Numbers indicated with * are from [41]. SPARE achieves a superior performance much faster. † We couldn't replicate DFR's result on CMNIST due to the lack of experimental details in the original paper, so we cite the only reported number for reference and leave other entries blank.

	Group Info	Train Cost	CMNIST		Waterbirds		CelebA	
			Worst-group	Average	Worst-group	Average	Worst-group	Average
ERM	×	1x	0.0* \pm 0.0	20.1* \pm 0.2	62.6* \pm 0.3	97.3* \pm 1.0	47.7* \pm 2.1	94.9* \pm 0.3
CB	×	1x	0.0 \pm 0.0	23.7 \pm 3.1	62.8 \pm 1.6	97.1 \pm 0.1	46.1 \pm 1.5	95.2 \pm 0.4
EIIL	×	1x	72.8* \pm 6.8	90.7* \pm 0.9	77.2* \pm 1.0	96.5* \pm 0.2	81.7* \pm 0.8	85.7* \pm 0.1
PGI	×	1x	73.5* \pm 1.8	88.5* \pm 1.4	79.5* \pm 1.9	95.5* \pm 0.8	85.3* \pm 0.3	87.3* \pm 0.1
GEORGE	×	2x	76.4* \pm 2.3	89.5* \pm 0.3	76.2* \pm 2.0	95.7* \pm 0.5	54.9* \pm 1.9	94.6* \pm 0.2
LfF	×	2x	0.0* \pm 0.0	25.0* \pm 0.5	78.0* \pm N/A	91.2* \pm N/A	77.2* \pm N/A	85.1* \pm N/A
CIM	×	2x	0.0* \pm 0.0	36.8* \pm 1.3	77.2* \pm N/A	95.6* \pm N/A	83.6* \pm N/A	90.6* \pm N/A
JTT	×	5x-6x	74.5* \pm 2.4	90.2* \pm 0.8	83.8* \pm 1.2	89.3* \pm 0.7	81.5* \pm 1.7	88.1* \pm 0.3
CnC	×	2x-12x	77.4* \pm 3.0	90.9* \pm 0.6	88.5* \pm 0.3	90.9* \pm 0.1	88.8* \pm 0.9	89.9* \pm 0.5
SPARE	×	1x	83.0\pm1.7	91.8\pm0.7	89.8\pm0.6	94.2\pm1.6	90.3\pm0.3	91.1\pm0.1
SSA	validation	1.5x-5x	0.0 \pm 0.0	47.9 \pm 14.4	89.0 \pm 0.6	92.2 \pm 0.9	89.8\pm1.3	92.8 \pm 0.1
DFR $_{Tr}^{Tr}$	training sub.	1x	-	-	90.4 \pm 1.5	94.1 \pm 0.5	80.1 \pm 1.1	89.7 \pm 0.4
DFR $_{Tr}^{Val}$	validation	1x	80.4 \pm 1.1	-	91.8\pm2.6	93.5 \pm 1.4	87.3 \pm 1.0	90.2 \pm 0.8
GB	training	1x	82.2\pm1.0	91.7 \pm 0.6	86.3 \pm 0.3	93.0 \pm 1.5	85.0 \pm 1.1	92.7 \pm 0.1
GDRO	training	1x	78.5 \pm 4.5	90.6 \pm 0.1	89.9* \pm 0.6	92.0* \pm 0.6	88.9* \pm 1.3	93.9* \pm 0.1

$\lambda = 1$. However, when clusters are not well separated (lower silhouette score), some examples from the majority group are spread in smaller clusters. In this case, sampling less from the large clusters is enough to balance the groups, as the majority groups are sampled when we upsample the small clusters. Here, we can balance the groups using $\lambda = 2$. Empirically, we found that $\lambda = 1$ or 2 is enough to effectively mitigate the spurious correlation in all our experiments. Note that our importance sampling method does not increase the size of the training data, and only changes the data distribution. Hence, it does not increase the training time. The pseudocode is illustrated in Alg. 1.

6 Experiments

In this section, we evaluate the effectiveness of SPARE in finding spurious correlations early in training, and eliminating while training on various spurious benchmark datasets. Then, we apply SPARE to discover and mitigate spurious correlations in Restricted ImageNet to confirm its broader applicability.

6.1 Mitigating Spurious Correlations in Benchmark Datasets

We first evaluate the effectiveness of SPARE in alleviating spurious correlations on spurious benchmarks. The reported results are averaged over three runs with different model initializations.

Datasets & Models. (1) CMNIST [2] contains colored handwritten digits derived from MNIST [15]. We follow the challenging 5-class setting in [41] where every two digits form one class and 99.5% of training examples in each class are spuriously correlated with a distinct color. We use a 5-layer CNN (LeNet-5 [15]) for CMNIST. (2) Waterbirds [28] contains two classes (landbird vs. waterbird) and the background (land or water) is the spurious feature. Majority groups are (waterbird, water) and (landbird, land). (3) CelebA [17] is another most commonly used benchmark for spurious correlations. Following [28], we consider the hair color (blond vs. non-blond) as the class labels and gender (male or female) as the spurious feature. The majority groups are (blond, female) and (non-blond male). For both Waterbirds and CelebA, we follow the standard settings used in the previous work to train a ResNet-50 model [10] pretrained on ImageNet provided by the Pytorch library [25]. More details about the datasets and the experimental settings can be found in Appendix C.

Baselines. We compare SPARE with the state-of-the-art methods for eliminating spurious correlations in Table 1, in terms of both worst-group accuracy, i.e., the minimum accuracy across all groups, and average accuracy. We use adjusted average accuracy for Waterbirds, i.e., the average accuracy over groups weighted by their size. This is consistent with prior work, and is done because the

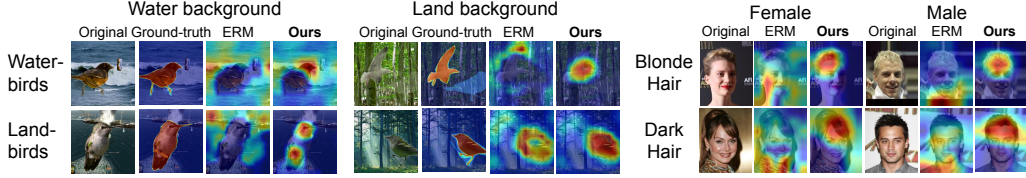


Figure 2: GradCAM Visualization. Warmer colors correspond to the pixels that are weighed more in making the final classification. SPARE allows learning the core features instead of spurious ones.

validation and test sets are group-balanced while the training set is skewed. GB (Group Balancing) and GDRO [28] use the group label of all training examples, and SSA [23] uses the group labels of the validation data. DFR [14] uses a group-balanced data drawn from either validation (DFR_{Tr}^{Tr}) or training (DFR_{Tr}^{Val}) data. The rest of the methods infer the group labels without using such information.

SPARE outperforms SOTA algorithms, including those that require group information. Table 1 shows that compared to baselines that do not use the group labels, SPARE obtains the *highest* worst-group accuracy, while maintaining high average accuracy. In particular, SPARE consistently outperforms the best baselines, CnC [41] and JTT [16], on worst-group and average accuracy while having up to 12x lower computational cost. Notably, SPARE performs comparably to those that use the group information, and even achieves a better worst-group accuracy on CMNIST and CelebA and has a comparable worst-group but higher average accuracy on the Waterbirds. Note that DFR_{Tr}^{Val} trains on group-balanced validation data, while SPARE does not. As group labels are unavailable in real-world datasets, methods that do not rely on group labels are more practical. Among such methods, SPARE has a superior performance and easily scales to large datasets. Notably, SPARE finds the groups, at epoch 2 for CMNIST and Waterbirds, and at epoch 1 for CelebA.

SPARE reaches SOTA performance under extreme group imbalance. Many state-of-the-art algorithms that can successfully eliminate spurious correlations in the Waterbirds and CelebA, severely fail on CMNIST, by providing as low as 0% worst-group accuracy. In CMNIST, every class has a very large majority and *four* very small minority groups, and there is a very strong spurious correlation between the color of the majority group and the corresponding class. Here, the small size of the minority groups makes it difficult to infer the groups based on loss (LFF [22]), data augmentation (CIM [35]), or semi-supervised learning (SSA [23]). Besides, state-of-the-art methods that partition every class into only two groups, namely EIL [6], PGI [1], CnC [41], and JTT [16], fail to balance the minority groups. This is because the minority groups need to be extensively upweighted or upsampled to make a balance with the majority group due to their small sizes, and extensive upweighting or upsampling them as a whole exaggerates the small differences between the original size of the minority groups and makes them imbalanced w.r.t. each other. This yields an inferior worst-group accuracy. In contrast, SPARE finds multiple minority clusters via silhouette analysis (see Figure 1c). By importance sampling from each cluster based on its size, SPARE can successfully balance the groups and achieve state-of-the-art worst-group and average accuracy.

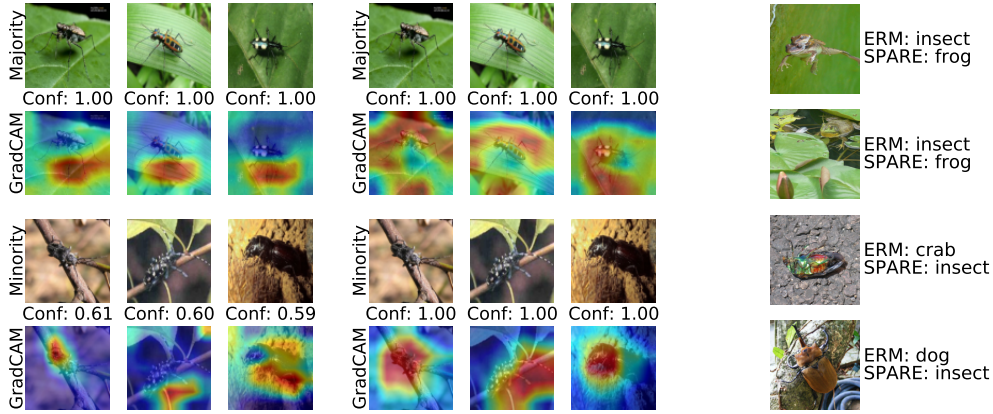
GradCAM. Fig. 2 compares GradCAM [31] visualizations depicting saliency maps for samples from Waterbirds with water and land backgrounds (left), and from CelebA with different genders (right), when ResNet50 is trained by ERM vs. SPARE. Warmer colors indicate the pixels that the model considered more important for making the final classification, based on gradient activations. We see that training with SPARE allows the model to learn the core feature, instead of the spurious features.

6.2 Ablation Studies

Next, we show that SPARE effectively separates majority and minority groups regardless of the network architecture early in training and explain how we determine cluster importance using silhouette scores without group information. **Network Structure.** First, we show SPARE can separate majority and minority groups independent of the network architecture, early

Table 2: Identifying groups in Waterbirds, based on the output of different networks early in training.

Model	Epoch	WG Acc	Avg Acc
RN18	4	89.5 \pm 0.8	96.6 \pm 0.3
RN50	4	89.1 \pm 2.1	95.9 \pm 0.7
Wide RN50	5	90.8 \pm 0.5	95.9 \pm 0.7
DenseNet121	5	89.3 \pm 1.5	96.3 \pm 0.6
Pretrained RN50	1	89.8 \pm 0.6	94.2 \pm 1.6



(a) Insects in ImageNet, Epoch 8. (b) Insects in ImageNet, End. (c) SPARE corrects spurious correlation.

Figure 3: Spurious correlation between "green leaf" & "insect" in Restricted ImageNet found by SPARE.

in training. To do so, we cluster output of ResNets of varying depths and widths, namely, ResNet-18, ResNet-50, Wide ResNet-50 [40], as well as DenseNet121 [13], and apply importance sampling to the clusters to train a pretrained ResNet-50 model on Waterbirds (same setting as in Table 1). Table 2 shows the worst-group and adjusted average accuracy. We see that all the networks can successfully separate the groups within the first 5 epochs. This confirms the effectiveness of simplicity bias in identifying groups in the early training phase. Details of the experiments can be found in Appendix C.

Importance Sampling Power (λ). Next, we explain how we determine the importance of different clusters using silhouette scores. Table 3 presents the average silhouette score for each class in different datasets. A higher average silhouette score indicates that clusters are well separated, such as in CMNIST and the female class in CelebA. This means we can accurately identify both the majority and minority groups. However, when clusters are not clearly separated (lower silhouette scores), some examples from the majority group get mixed up with the smaller clusters. As a result, we sample even fewer examples from the larger clusters. When clusters are well separated, we use $\lambda = 1$ to ensure equal treatment of groups. However, for less separable clusters, using $\lambda = 2$ helps achieve group balance.

Table 3: Average Silhouette scores of clusters in different classes, and the corresponding importance sampling power (λ) used for each class.

Dataset	Silhouette score	Sampling power (λ)
CMNIST	between 0.991-0.997	[1, 1, 1, 1, 1]
Waterbirds	[0.886, 0.758]	[2, 2]
CelebA	[0.924, 0.757]	[1, 2]

6.3 Discovering and Mitigating Spurious Correlations in Restricted ImageNet

Finally, we show the applicability of SPARE to discover and mitigate spurious correlations in more realistic settings. We use Restricted ImageNet [35], a 9-superclass subset of ImageNet, to train ResNet-50 from scratch. We applied SPARE to cluster the model’s output in the first 10 epochs, and inspected the clusters as described below. However, we found that the results are not very sensitive to the choice of the initial epoch. See Appendix D for more details on the dataset and experiment.

Frog vs. Insect. By inspecting the clusters with the highest fraction of misclassified examples to another class, we find that many Frog images are misclassified as Insects. Figure 3a shows examples from the two groups SPARE finds for the Insect class at epoch 8. GradCAM reveals an obvious spurious correlation between “green leaf” and the insect class that is maintained until the end of the training, as illustrated in Figure 3b. We also observe a large gap between the confidence of examples in the two groups. This indicates that the model has learned the spurious feature early in training.

Next, we apply importance sampling with $\lambda = 2$ (silhouette score < 0.9), to alleviate the spurious correlation. Here, as the underlying group labels are not available, GroupDRO and GB are not applicable. Besides, state-of-the-art methods such as JTT and CnC are prohibitively slow to apply to ImageNet (see training cost in Table 1). Hence, we only

Table 4: Mitigating spurious in Restricted ImageNet.

	Test Acc	Insect Minority	Frog Minority
ERM	96.0%	83.3%	96.2%
CB	95.9%	87.5% \uparrow	96.2% $-$
EIIL	93.1%	76.0% \downarrow	90.4% \downarrow
SPARE	95.4%	86.3% \uparrow	98.1% \uparrow

compare SPARE with Class Balancing (CB) and EIIL. Table 4 shows that SPARE can successfully improve the accuracy of both insect and frog minorities by 3% and 2% respectively, with the slightest drop in the total accuracy. Note that examples in Frog minority group were classified as Insect, due to “green leaf” in their background. Figure 3c shows examples of Frog and Insect minorities that are correctly classified after training with SPARE. In contrast, CB improves the accuracy only on Insect minority. Note that while CB upsamples both classes, it cannot improve the accuracy on Frog minority examples that are misclassified as Insect due to the spurious correlation. We also see that EIIL drops the accuracy on minorities as well as the total accuracy. This is mainly because EIIL separates and upweights many examples that are misclassified by ERM, as we report in Appendix D. Extensive upweighting of such examples harms the performance. We expect this effect to be even more severe for methods like JTT, which directly find the misclassified examples as the minority group. In contrast, SPARE better separates the groups and mitigates the spurious correlation by balancing them.

7 Conclusion

In this work, we studied how simple spurious features are learned during training neural networks with gradient methods. In particular, we analyzed a two-layer fully-connected neural network and showed that large groups of examples with spurious features are separable based on the model’s output, early in training. If spurious features have a small enough noise-to-signal ratio, the network’s output on a large number of examples will be almost exclusively determined by the spurious features and will be nearly invariant to the core features. Based on the above theoretical insights, we proposed SPARE, that separates majority and minority groups by clustering the model output early in training. Then, it applies importance sampling based on the cluster sizes to make the groups relatively balanced. We showed that our method achieves state-of-the-art worst-group accuracy on various datasets, and is highly scalable. We also demonstrated the applicability of SPARE in more realistic settings, to discover and mitigate spurious correlations from Restricted ImageNet.

Limitations. To our knowledge, simplicity bias has been mainly studied for vision models, and applicability of our method to other data modalities requires further investigations. Our method promotes fairness and equity in machine learning and we are not aware of any potential negative social impact.

References

- [1] Ahmed, F., Bengio, Y., van Seijen, H., and Courville, A. Systematic generalisation with group invariant predictions. In *International Conference on Learning Representations*, 2020.
- [2] Alain, G., Lamb, A., Sankar, C., Courville, A., and Bengio, Y. Variance reduction in sgd by distributed importance sampling. *arXiv preprint arXiv:1511.06481*, 2015.
- [3] Arjovsky, M. and Bottou, L. Towards principled methods for training generative adversarial networks. *arXiv preprint arXiv:1701.04862*, 2017.
- [4] Badanidiyuru, A., Mirzasoleiman, B., Karbasi, A., and Krause, A. Streaming submodular maximization: Massive data summarization on the fly. In *Proceedings of the 20th ACM SIGKDD international conference on Knowledge discovery and data mining*, pp. 671–680, 2014.
- [5] Byrd, J. and Lipton, Z. What is the effect of importance weighting in deep learning? In *International Conference on Machine Learning*, pp. 872–881. PMLR, 2019.
- [6] Creager, E., Jacobsen, J.-H., and Zemel, R. Environment inference for invariant learning. In *International Conference on Machine Learning*, pp. 2189–2200. PMLR, 2021.
- [7] Cui, Y., Jia, M., Lin, T.-Y., Song, Y., and Belongie, S. Class-balanced loss based on effective number of samples. In *Proceedings of the IEEE/CVF conference on computer vision and pattern recognition*, pp. 9268–9277, 2019.
- [8] Goyal, P., Dollár, P., Girshick, R., Noordhuis, P., Wesolowski, L., Kyrola, A., Tulloch, A., Jia, Y., and He, K. Accurate, large minibatch sgd: Training imagenet in 1 hour. *arXiv preprint arXiv:1706.02677*, 2017.

- [9] He, H. and Garcia, E. A. Learning from imbalanced data. *IEEE Transactions on knowledge and data engineering*, 21(9):1263–1284, 2009.
- [10] He, K., Zhang, X., Ren, S., and Sun, J. Deep residual learning for image recognition. In *Proceedings of the IEEE conference on computer vision and pattern recognition*, pp. 770–778, 2016.
- [11] Hermann, K. and Lampinen, A. What shapes feature representations? exploring datasets, architectures, and training. *Advances in Neural Information Processing Systems*, 33:9995–10006, 2020.
- [12] Hu, W., Xiao, L., Adlam, B., and Pennington, J. The surprising simplicity of the early-time learning dynamics of neural networks. *Advances in Neural Information Processing Systems*, 33: 17116–17128, 2020.
- [13] Huang, G., Liu, Z., Van Der Maaten, L., and Weinberger, K. Q. Densely connected convolutional networks. In *Proceedings of the IEEE conference on computer vision and pattern recognition*, pp. 4700–4708, 2017.
- [14] Kirichenko, P., Izmailov, P., and Wilson, A. G. Last layer re-training is sufficient for robustness to spurious correlations. In *The Eleventh International Conference on Learning Representations*, 2023. URL <https://openreview.net/forum?id=Zb6c8A-Fghk>.
- [15] LeCun, Y., Bottou, L., Bengio, Y., and Haffner, P. Gradient-based learning applied to document recognition. *Proceedings of the IEEE*, 86(11):2278–2324, 1998.
- [16] Liu, E. Z., Haghighi, B., Chen, A. S., Raghunathan, A., Koh, P. W., Sagawa, S., Liang, P., and Finn, C. Just train twice: Improving group robustness without training group information. In *International Conference on Machine Learning*, pp. 6781–6792. PMLR, 2021.
- [17] Liu, Z., Luo, P., Wang, X., and Tang, X. Deep learning face attributes in the wild. In *Proceedings of International Conference on Computer Vision (ICCV)*, December 2015.
- [18] Mirzasoleiman, B., Karbasi, A., Sarkar, R., and Krause, A. Distributed submodular maximization: Identifying representative elements in massive data. In *Advances in Neural Information Processing Systems*, pp. 2049–2057, 2013.
- [19] Mirzasoleiman, B., Badanidiyuru, A., Karbasi, A., Vondrák, J., and Krause, A. Lazier than lazy greedy. In *Twenty-Ninth AAAI Conference on Artificial Intelligence*, 2015.
- [20] Nagarajan, V., Andreassen, A., and Neyshabur, B. Understanding the failure modes of out-of-distribution generalization. *arXiv preprint arXiv:2010.15775*, 2020.
- [21] Nakkiran, P., Kaplun, G., Kalimeris, D., Yang, T., Edelman, B. L., Zhang, F., and Barak, B. Sgd on neural networks learns functions of increasing complexity. In *Proceedings of the 33rd International Conference on Neural Information Processing Systems*, pp. 3496–3506, 2019.
- [22] Nam, J., Cha, H., Ahn, S., Lee, J., and Shin, J. Learning from failure: De-biasing classifier from biased classifier. *Advances in Neural Information Processing Systems*, 33:20673–20684, 2020.
- [23] Nam, J., Kim, J., Lee, J., and Shin, J. Spread spurious attribute: Improving worst-group accuracy with spurious attribute estimation. In *International Conference on Learning Representations*, 2021.
- [24] Neyshabur, B., Tomioka, R., and Srebro, N. In search of the real inductive bias: On the role of implicit regularization in deep learning. *arXiv preprint arXiv:1412.6614*, 2014.
- [25] Paszke, A., Gross, S., Massa, F., Lerer, A., Bradbury, J., Chanan, G., Killeen, T., Lin, Z., Gimelshein, N., Antiga, L., Desmaison, A., Kopf, A., Yang, E., DeVito, Z., Raison, M., Tejani, A., Chilamkurthy, S., Steiner, B., Fang, L., Bai, J., and Chintala, S. Pytorch: An imperative style, high-performance deep learning library. In Wallach, H., Larochelle, H., Beygelzimer, A., d'Alché-Buc, F., Fox, E., and Garnett, R. (eds.), *Advances in Neural Information Processing Systems 32*, pp. 8024–8035. 2019.

- [26] Pezeshki, M., Kaba, O., Bengio, Y., Courville, A. C., Precup, D., and Lajoie, G. Gradient starvation: A learning proclivity in neural networks. *Advances in Neural Information Processing Systems*, 34:1256–1272, 2021.
- [27] Rousseeuw, P. J. Silhouettes: a graphical aid to the interpretation and validation of cluster analysis. *Journal of computational and applied mathematics*, 20:53–65, 1987.
- [28] Sagawa, S., Koh, P. W., Hashimoto, T. B., and Liang, P. Distributionally robust neural networks. In *International Conference on Learning Representations*, 2019.
- [29] Sagawa, S., Raghunathan, A., Koh, P. W., and Liang, P. An investigation of why overparameterization exacerbates spurious correlations. In *International Conference on Machine Learning*, pp. 8346–8356. PMLR, 2020.
- [30] Sandler, M., Howard, A., Zhu, M., Zhmoginov, A., and Chen, L.-C. Mobilenetv2: Inverted residuals and linear bottlenecks. In *Proceedings of the IEEE conference on computer vision and pattern recognition*, pp. 4510–4520, 2018.
- [31] Selvaraju, R. R., Cogswell, M., Das, A., Vedantam, R., Parikh, D., and Batra, D. Grad-cam: Visual explanations from deep networks via gradient-based localization. In *Proceedings of the IEEE international conference on computer vision*, pp. 618–626, 2017.
- [32] Shah, H., Tamuly, K., Raghunathan, A., Jain, P., and Netrapalli, P. The pitfalls of simplicity bias in neural networks. *Advances in Neural Information Processing Systems*, 33:9573–9585, 2020.
- [33] Shimodaira, H. Improving predictive inference under covariate shift by weighting the log-likelihood function. *Journal of statistical planning and inference*, 90(2):227–244, 2000.
- [34] Sohoni, N., Dunnmon, J., Angus, G., Gu, A., and Ré, C. No subclass left behind: Fine-grained robustness in coarse-grained classification problems. *Advances in Neural Information Processing Systems*, 33:19339–19352, 2020.
- [35] Taghanaki, S. A., Choi, K., Khasahmadi, A. H., and Goyal, A. Robust representation learning via perceptual similarity metrics. In *International Conference on Machine Learning*, pp. 10043–10053. PMLR, 2021.
- [36] Teney, D., Abbasnejad, E., Lucey, S., and Van den Hengel, A. Evading the simplicity bias: Training a diverse set of models discovers solutions with superior ood generalization. In *Proceedings of the IEEE/CVF Conference on Computer Vision and Pattern Recognition*, pp. 16761–16772, 2022.
- [37] Tsipras, D., Santurkar, S., Engstrom, L., Turner, A., and Madry, A. Robustness may be at odds with accuracy. In *International Conference on Learning Representations*, 2019. URL <https://openreview.net/forum?id=SyxAb30cY7>.
- [38] Wah, C., Branson, S., Welinder, P., Perona, P., and Belongie, S. Technical Report CNS-TR-2011-001, California Institute of Technology, 2011.
- [39] Wolsey, L. A. An analysis of the greedy algorithm for the submodular set covering problem. *Combinatorica*, 2(4):385–393, 1982.
- [40] Zagoruyko, S. and Komodakis, N. Wide residual networks. In *British Machine Vision Conference 2016*. British Machine Vision Association, 2016.
- [41] Zhang, M., Sohoni, N. S., Zhang, H. R., Finn, C., and Ré, C. Correct-n-contrast: A contrastive approach for improving robustness to spurious correlations. *arXiv preprint arXiv:2203.01517*, 2022.

A Appendix

A.1 Simplicity Bias

A recent body of work revealed that the neural network trained with (stochastic) gradient methods can be approximated on the training data by a linear function early in training [11, 12, 21, 24, 26, 32]. We hypothesize that a slightly stronger statement holds, namely the approximation still holds if we isolate a core or spurious feature from an example and input it to the model.

Assumption A.1 (simplicity bias on core and spurious features, informal). Suppose that f^{lin} is a linear function that closely approximates $f(\mathbf{x}; \mathbf{W}, \mathbf{z})$ on the training data. Then f^{lin} also approximates f on input either a core feature or a spurious feature corresponding to a majority group in some class, that is

$$\begin{aligned} f^{lin}(\mathbf{v}_c) &\approx f(\mathbf{v}_c; \mathbf{W}, \mathbf{z}) & \forall c \in \mathcal{C} \\ f^{lin}(\mathbf{v}_s) &\approx f(\mathbf{v}_s; \mathbf{W}, \mathbf{z}) & \forall s \in \mathcal{A} \end{aligned}$$

Intuitively, every core feature and every spurious feature corresponding to a majority group is well represented in the training dataset, and since it is known that the linear model and the full neural network agree on the training dataset, we can expect them to agree on such features as well. Note that spurious features that do not appear in majority groups may not be well represented in the training dataset, hence we do not require that the linear model approximates the neural network well on such features. The formal statement is provided below as Assumption A.6.

A.2 Setting

We now introduce the formal mathematical setting for the theory.

Let $\mathcal{D} = \{(\mathbf{x}_i, y_i)\}_{i=1}^n \subset \mathbb{R}^d \times \mathbb{R}$, be a dataset with covariance Σ . Define the data matrix $\mathbf{X} = [\mathbf{x}_1 \ \dots \ \mathbf{x}_n]^\top$ and the label vector $\mathbf{y} = [y_1 \ \dots \ y_n]^\top$. We use $\|\cdot\|$ to refer to the Euclidean norm of a vector or the spectral norm of the data.

Following Hu et al. 12, we make the following assumptions:

Assumption A.2 (input distribution). The data has the following properties (with high probability):

$$\begin{aligned} \frac{\|\mathbf{x}_i\|^2}{d} &= 1 \pm O\left(\sqrt{\frac{\log n}{d}}\right), \forall i \in [n] \\ \frac{|\langle \mathbf{x}_i, \mathbf{x}_j \rangle|}{d} &= O\left(\sqrt{\frac{\log n}{d}}\right), \forall i, j \in [n], i \neq j \\ \|\mathbf{X} \mathbf{X}^\top\| &= \Theta(n) \end{aligned}$$

Assumption A.3 (activation function). The activation $\phi(\cdot)$ satisfies either of the following:

- smooth activation: ϕ has bounded first and second derivative
- piecewise linear activation:

$$\phi(z) = \begin{cases} z & z \geq 0 \\ az & z < 0 \end{cases}$$

Assumption A.4 (initialization). The weights (\mathbf{W}, \mathbf{v}) are initialized using symmetric initialization:

$$\begin{aligned} \mathbf{w}_1, \dots, \mathbf{w}_{\frac{m}{2}} &\sim \mathcal{N}(\mathbf{0}_d, \mathbf{I}_d), & \mathbf{w}_{i+\frac{m}{2}} &= \mathbf{w}_i (\forall i \in 1, \dots, \frac{m}{2}) \\ v_1, \dots, v_{\frac{m}{2}} &\sim \text{Unif}(\{-1, 1\}), & v_{i+\frac{m}{2}} &= -v_i (\forall i \in 1, \dots, \frac{m}{2}) \end{aligned}$$

It is not hard to check that the concrete scenario we choose in our analysis satisfies the above assumptions. Now, given the following assumptions, we leverage the result of Hu et al. [12]:

Theorem A.5 (Hu et al. 12). Let $\alpha \in (0, 1/4)$ be a fixed constant. Suppose d is the input dimensionality, $\frac{\langle \mathbf{x}_i, \mathbf{x}_j \rangle}{d} = \mathbb{1}_{i=j} \pm O\left(\sqrt{\frac{\log n}{d}}\right), \forall i, j \in [n]$, the data matrix $\mathbf{X} = \{\mathbf{x}_i\}_{i=1}^n$ has spectral norm

$\|\mathbf{X}\mathbf{X}^\top\| = \Theta(n)$, and for the labels we have $|y_i| \leq 1 \forall y_i$. Assume the number of training samples n and the network width m satisfy $n, m = \Omega(d^{1+\alpha})$, $n, m \leq d^{\mathcal{O}(1)}$, and the learning rate $\eta \ll d$. Then, there exist a universal constant C , such that with high probability for all $0 \leq t \leq T = C \cdot \frac{d \log d}{\eta}$, the network $f(\mathbf{w}_t, \mathbf{X})$ trained with GD is very close to a linear function $f^{lin}(\boldsymbol{\beta}, \mathbf{X})$:

$$\frac{1}{n} \sum_{i=1}^n (f^{lin}(\boldsymbol{\beta}_t, \mathbf{X}) - f(\mathbf{w}_t, \mathbf{X}))^2 \leq \frac{\eta^2 t^2}{d^{2+\Omega(\alpha)}} \leq \frac{1}{d^{\Omega(\alpha)}}. \quad (11)$$

In particular, the linear model $f^{lin}(\boldsymbol{\beta}, \mathbf{X})$ takes operates on the transformed data $\boldsymbol{\psi}(\mathbf{x})$, where

$$\begin{aligned} \boldsymbol{\psi}(\mathbf{x}) &= \begin{bmatrix} \sqrt{\frac{2}{d}} \zeta \mathbf{x} \\ \sqrt{\frac{3}{2d}} \nu \\ \vartheta_0 + \vartheta_1 \left(\frac{\|\mathbf{x}\|}{\sqrt{d}} - 1 \right) + \vartheta_2 \left(\frac{\|\mathbf{x}\|}{\sqrt{d}} - 1 \right)^2 \end{bmatrix} \\ \zeta &= \mathbb{E}_{g \sim \mathcal{N}(0,1)} [\phi'(g)] \\ \nu &= \mathbb{E}_{g \sim \mathcal{N}(0,1)} [g \phi'(g)] \sqrt{\frac{\text{Tr}[\boldsymbol{\Sigma}^2]}{d}} \\ \vartheta_0 &= \mathbb{E}_{g \sim \mathcal{N}(0,1)} [g] \\ \vartheta_1 &= \mathbb{E}_{g \sim \mathcal{N}(0,1)} [g \phi'(g)] \\ \vartheta_2 &= \mathbb{E}_{g \sim \mathcal{N}(0,1)} \left[\left(\frac{1}{2} g^3 - g \right) \phi'(g) \right] \end{aligned}$$

Note that $\boldsymbol{\psi}(\mathbf{x})$ consists of a scaled version of the data, a bias term, and a term that depends on the norm of the example. We will adopt the notation $f(\boldsymbol{\psi}; \boldsymbol{\beta}) = \boldsymbol{\psi}^\top \boldsymbol{\beta}$ for the linear model.

We can now formally state A.1:

Assumption A.6 (formal version of A.1). Suppose that Theorem A.5 holds. Then with high probability, for all such t the following also holds for all $c \in \mathcal{C}$ and for all $s \in \mathcal{A}$:

$$\begin{aligned} |f^{lin}(\boldsymbol{\beta}_t, \mathbf{v}_c) - f(\mathbf{w}_t, \mathbf{v}_c)| &\leq \frac{\eta t}{d^{1+\Omega(\alpha)}}, \\ |f^{lin}(\boldsymbol{\beta}_t, \mathbf{v}_s) - f(\mathbf{w}_t, \mathbf{v}_s)| &\leq \frac{\eta t}{d^{1+\Omega(\alpha)}}. \end{aligned}$$

We will assume the former holds in the proof of the following theorems, although as we will see the assumption is unnecessary for Theorem 4.2.

B Proof for Theorems

B.1 Notation

For the analysis, we split $\boldsymbol{\beta}$ into its components corresponding to the data, bias and norm parts of $\boldsymbol{\psi}$;

that is $\boldsymbol{\beta} = \begin{pmatrix} \boldsymbol{\beta}' \\ \beta_{bias} \\ \beta_{norm} \end{pmatrix}$ for $\boldsymbol{\beta}' \in \mathbb{R}^d$, $\beta_{bias} \in \mathbb{R}$, $\beta_{norm} \in \mathbb{R}$. We use the inner product between $\boldsymbol{\beta}'$

and a feature \mathbf{v} to understand how well the linear model learns a feature $\mathbf{v} \in \mathbb{R}^d$. With slight abuse of notation, we will simply write $\langle \boldsymbol{\beta}, \mathbf{v} \rangle$ to mean $\langle \boldsymbol{\beta}', \mathbf{v} \rangle$.

We also define the matrix $\boldsymbol{\Phi} = [\phi_1 \ \dots \ \phi_n]^\top$.

B.2 Proof of Theorem 4.1 and 4.2

Theorem 4.1. Let $\alpha \in (0, \frac{1}{4})$ be a fixed constant. Suppose the number of training samples n and the network width m satisfy $n \gtrsim d^{1+\alpha}$ and $m \gtrsim d^{1+\alpha}$. Let n_c be the number of examples in class c , and

$n_{c,s} = |g_{c,s}|$ be the size of group $g_{c,s}$ with label c and spurious feature $\mathbf{v}_s \in \mathcal{A}$. Then, under the setting of Sec. 3 there exist a constant $\nu_1 > 0$, such that with high probability, for all $0 \leq t \leq \nu_1 \cdot \sqrt{\frac{d^{1-\alpha}}{\eta}}$, the contribution of the core and spurious features to the network output can be quantified as follows:

$$f(\mathbf{v}_c; \mathbf{W}_t, \mathbf{z}_t) = \sqrt{\frac{2}{d}} \eta \zeta c \|\mathbf{v}_c\|^2 t \left(\frac{n_c}{n} \pm \mathcal{O}(d^{-\Omega(\alpha)}) \right), \quad (5)$$

$$f(\mathbf{v}_s; \mathbf{W}_t, \mathbf{z}_t) = \sqrt{\frac{2}{d}} \eta \zeta c \|\mathbf{v}_s\|^2 t \left(\frac{n_{c,s} - n_{c',s}}{n} \pm \mathcal{O}(d^{-\Omega(\alpha)}) \right), \quad (6)$$

where $c' = \mathcal{C} \setminus c$, and ζ is the expected gradient of activation functions at random initialization.

Corollary 4.2 (Separability of majority and minority groups). Suppose that for all classes, a majority group has at least K examples and a minority group has at most k examples. Then, under the assumptions of Theorem 4.1, examples in the majority and minority groups are separable based on the model's output, early in training. That is, for all $0 \leq t \leq \nu_1 \cdot \sqrt{\frac{d^{1-\alpha}}{\eta}}$, with high probability, the following holds for at least $1 - \mathcal{O}(d^{-\Omega(\alpha)})$ fraction of the training examples \mathbf{x}_i in group $g_{c,s}$:

If $g_{c,s}$ is in a majority group in class $c = 1$:

$$f(\mathbf{x}_i; \mathbf{W}_t, \mathbf{z}_t) \geq \frac{2\eta\zeta^2 t}{d} \left(\frac{\|\mathbf{v}_s\|^2 (K - k)}{n} + \xi \pm \mathcal{O}(d^{-\Omega(\alpha)}) \right) + \rho(t, \phi, \Sigma), \quad (7)$$

If $g_{c,s}$ is in a minority group in class $c = 1$, but $g_{c',s}$ is a majority group in class $c' = -1$:

$$f(\mathbf{x}_i; \mathbf{W}_t, \mathbf{z}_t) \leq \frac{2\eta\zeta^2 t}{d} \left(-\frac{\|\mathbf{v}_s\|^2 (K - k)}{n} + \xi \pm \mathcal{O}(d^{-\Omega(\alpha)}) \right) + \rho(t, \phi, \Sigma), \quad (8)$$

where ρ is constant for all examples in the same class, $\xi \sim \mathcal{N}(0, \kappa)$ with $\kappa = \frac{1}{n} (\sum_c n_c^2 \sigma_c^2 \|\mathbf{v}_c\|^2)^{1/2} + \frac{1}{n} (\sum_s (n_{c,s} - n_{c',s})^2 \sigma_s^2 \|\mathbf{v}_s\|^2)^{1/2}$ is the total effect of noise on the model.

Analogous statements holds for the class $c = -1$ by changing the sign and direction of the inequality.

As in [12], we will conduct our analysis under the high probability events that $\|\Psi^\top \Psi\| = \mathcal{O}(\frac{n}{d})$ and for all training data \mathbf{x} , $\frac{\|\mathbf{x}\|}{\sqrt{d}} = 1 \pm \mathcal{O}(\sqrt{\frac{\log n}{d}})$.

Starting from the rule of gradient descent

$$\begin{aligned} \beta(t+1) &= \beta(t) - \frac{\eta}{n} \Psi^\top (\Psi \beta(t) - \mathbf{y}) \\ &= \left(I - \frac{\eta}{n} \Psi^\top \Psi \right) \beta(t) + \frac{\eta}{n} \Psi^\top \mathbf{y} \end{aligned}$$

Let $\mathbf{A} = I - \frac{\eta}{n} \Psi^\top \Psi$, $\mathbf{b} = \frac{\eta}{n} \Psi^\top \mathbf{y}$. Also, \mathbf{A} can be diagonalized as $\mathbf{A} = \mathbf{V} \mathbf{D} \mathbf{V}^\top$. Since $\|\Psi^\top \Psi\| = \mathcal{O}(\frac{n}{d})$, the eigenvalues of \mathbf{A} , call them $\lambda_1, \dots, \lambda_d$, are of order $1 - \mathcal{O}(\frac{n}{d})$. For $t \geq 1$, the previous recurrence relation admits the solution

$$\begin{aligned} \beta(t) &= (\mathbf{I} + \mathbf{A} + \dots + \mathbf{A}^{t-1}) \mathbf{b} \\ &= \mathbf{V} (\mathbf{I} + \mathbf{D} + \dots + \mathbf{D}^{t-1}) \mathbf{V}^\top \mathbf{b} \end{aligned}$$

When $t = \mathcal{O}(\sqrt{\frac{d^{1-\alpha}}{\eta}})$, the eigenvalues of $\mathbf{I} + \mathbf{D} + \dots + \mathbf{D}^{t-1}$ are on the order of

$$\begin{aligned} 1 + \lambda_i + \dots + \lambda_i^{t-1} &= \frac{1 - \lambda_i^t}{1 - \lambda_i} \\ &= 1 + \mathcal{O}(d^{-\frac{\alpha}{2}}) \end{aligned}$$

Thus we can approximate $\mathbf{I} + \mathbf{D} + \dots + \mathbf{D}^{t-1} = t\mathbf{I} + \mathbf{\Delta}$, where $\|\mathbf{\Delta}\| = \mathcal{O}(d^{-\frac{\alpha}{2}})$. Then

$$\beta(t) = \mathbf{V} (t\mathbf{I} + \mathbf{\Delta}) \mathbf{V}^\top \mathbf{b} = t\mathbf{b} + \mathbf{\Delta}_1 \mathbf{b}$$

where $\mathbf{\Delta}_1 = \mathbf{V} \mathbf{\Delta} \mathbf{V}^\top$ also satisfies $\|\mathbf{\Delta}_1\| = \mathcal{O}(d^{-\frac{\alpha}{2}})$.

From here we may calculate the following: the alignment of β with a core feature \mathbf{v}_c is

$$\langle \mathbf{v}_c, \beta \rangle = \sqrt{\frac{2}{d}} \frac{\eta \zeta c \|\mathbf{v}_c\|}{n} (t \pm O(d^{-\frac{\alpha}{2}})) (\|\mathbf{v}_c\| n_c \pm O(\sigma_c \sqrt{n})) \quad (12)$$

$$= \sqrt{\frac{2}{d}} \eta \zeta c \|\mathbf{v}_c\|^2 t \left(\frac{n_c}{n} \pm O(d^{-\Omega(\alpha)}) \right) \quad (13)$$

and the alignment with a spurious feature \mathbf{v}_s is

$$\langle \mathbf{v}_s, \beta \rangle = \sqrt{\frac{2}{d}} \frac{\eta \zeta c \|\mathbf{v}_s\|}{n} (t \pm O(d^{-\frac{\alpha}{2}})) (\|\mathbf{v}_s\| (n_{c,s} - n_{c',s}) \pm O(\sigma_s \sqrt{n})) \quad (14)$$

$$= \sqrt{\frac{2}{d}} \eta \zeta c \|\mathbf{v}_s\|^2 t \left(\frac{n_{c,s} - n_{c',s}}{n} \pm O(d^{-\Omega(\alpha)}) \right) \quad (15)$$

The effect of the noise is captured by the $O(\sigma \sqrt{n})$ terms, following standard concentration inequalities, and we used the fact that $\frac{1}{\sqrt{n}} = O(d^{-\Omega(\alpha)})$. The result transfers to the full neural network under assumption A.6, namely

$$f(\mathbf{v}_c; \mathbf{W}_t, \mathbf{z}_t) = \sqrt{\frac{2}{d}} \eta \zeta c \|\mathbf{v}_c\|^2 t \left(\frac{n_c}{n} \pm O(d^{-\Omega(\alpha)}) \right), \quad (16)$$

$$f(\mathbf{v}_s; \mathbf{W}_t, \mathbf{z}_t) = \sqrt{\frac{2}{d}} \eta \zeta c \|\mathbf{v}_s\|^2 t \left(\frac{n_{c,s} - n_{c',s}}{n} \pm O(d^{-\Omega(\alpha)}) \right), \quad (17)$$

This proves Theorem 4.1.

In addition, we calculate that

$$\beta_{norm}(t) = (tI + \Delta_1) \sum_{i=1}^n y_i \left(\vartheta_0 + \vartheta_1 \left(\frac{\|\mathbf{x}_i\|}{\sqrt{d}} - 1 \right) + \vartheta_2 \left(\frac{\|\mathbf{x}_i\|}{\sqrt{d}} - 1 \right)^2 \right) = O\left(\frac{\eta t}{\sqrt{n}}\right)$$

Then for the predictions at time t for an example in class $c = 1$, group $g_{1,s}$:

$$\begin{aligned} \psi(\mathbf{x})^\top \beta(t) &= \sqrt{\frac{2}{d}} \zeta \mathbf{x}^\top \beta' + \sqrt{\frac{3}{2d}} \nu \beta_{bias}(t) + \beta_{norm}(t) \left(\vartheta_0 + \vartheta_1 \left(\frac{\|\mathbf{x}\|}{\sqrt{d}} - 1 \right) + \vartheta_2 \left(\frac{\|\mathbf{x}\|}{\sqrt{d}} - 1 \right)^2 \right) \\ &= \sqrt{\frac{2}{d}} \zeta (\mathbf{v}_1 + \mathbf{v}_s + \boldsymbol{\xi})^\top \beta' + \sqrt{\frac{3}{2d}} \nu \beta_{bias}(t) + \vartheta_0 \beta_{norm}(t) \pm O\left(\eta t \sqrt{\frac{\log n}{nd}}\right) \end{aligned}$$

We have a few cases

1. $g_{1,k}$ is a majority group. In this case

$$\begin{aligned} \psi(\mathbf{x})^\top \beta(t) &\geq \frac{2\eta \zeta^2 t}{d} \left(\frac{n_1 \|\mathbf{v}_c\|^2}{n} + \frac{\|\mathbf{v}_s\|^2 (K - k)}{n} + \left\langle \boldsymbol{\xi}, \frac{1}{n} \mathbf{X}^\top \mathbf{y} \right\rangle \pm O(d^{-\Omega(\alpha)}) \right) \\ &\quad + \sqrt{\frac{3}{2d}} \nu \beta_{bias}(t) + \vartheta_0 \beta_{norm}(t) \pm O\left(\eta t \sqrt{\frac{\log n}{nd}}\right) \end{aligned}$$

2. $g_{1,k}$ is a minority group and $g_{-1,k}$ is a majority group. In this case

$$\begin{aligned} \psi(\mathbf{x})^\top \beta(t) &\leq \frac{2\eta \zeta^2 t}{d} \left(\frac{n_1 \|\mathbf{v}_c\|^2}{n} - \frac{\|\mathbf{v}_s\|^2 (K - k)}{n} + \left\langle \boldsymbol{\xi}, \frac{1}{n} \mathbf{X}^\top \mathbf{y} \right\rangle \pm O(d^{-\Omega(\alpha)}) \right) \\ &\quad + \sqrt{\frac{3}{2d}} \nu \beta_{bias}(t) + \vartheta_0 \beta_{norm}(t) \pm O\left(\eta t \sqrt{\frac{\log n}{nd}}\right) \end{aligned}$$

3. $g_{1,k}$ is such that no majority groups have the spurious feature. In this case

$$\begin{aligned} \psi(\mathbf{x})^\top \beta(t) &= \frac{2\eta \zeta^2 t}{d} \left(\frac{n_1 \|\mathbf{v}_c\|^2}{n} + \frac{\|\mathbf{v}_s\|^2 \tilde{k}}{n} + \left\langle \boldsymbol{\xi}, \frac{1}{n} \mathbf{X}^\top \mathbf{y} \right\rangle \pm O(d^{-\Omega(\alpha)}) \right) \\ &\quad + \sqrt{\frac{3}{2d}} \nu \beta_{bias}(t) + \vartheta_0 \beta_{norm}(t) \pm O\left(\eta t \sqrt{\frac{\log n}{nd}}\right), \quad |\tilde{k}| \leq k \end{aligned}$$

Now

$$\left\langle \boldsymbol{\xi}, \frac{1}{n} \mathbf{X}^\top \mathbf{y} \right\rangle = \sum_{c \in \{\pm 1\}} \frac{\|\mathbf{v}_c\| n_c}{n} \langle \boldsymbol{\xi}, \mathbf{v}_c \rangle + \sum_s \frac{\|\mathbf{v}_s\| (n_{1,s} - n_{-1,s})}{n} \langle \boldsymbol{\xi}, \mathbf{v}_s \rangle + \left\langle \boldsymbol{\xi}, \frac{1}{n} \sum_{i=1}^n \boldsymbol{\xi}_i y_i \right\rangle \quad (18)$$

$$= \sum_{c \in \{\pm 1\}} \frac{\|\mathbf{v}_c\| n_c}{n} \langle \boldsymbol{\xi}, \mathbf{v}_c \rangle + \sum_s \frac{\|\mathbf{v}_s\| (n_{1,s} - n_{-1,s})}{n} \langle \boldsymbol{\xi}, \mathbf{v}_s \rangle \pm O\left(\sqrt{\frac{d}{n}}\right) \quad (19)$$

$$\sim \mathcal{N}(0, \kappa) \pm O(d^{-\Omega(\alpha)}) \quad (20)$$

Finally, observe that $O\left(\eta t \sqrt{\frac{\log n}{nd}}\right) = O(d^{-1-\Omega(\alpha)})$. Combining all these results and setting

$\rho_1 = \frac{2\eta\zeta^2 ct}{d}, \rho_2 = \frac{\rho_1 n_1 \|\mathbf{v}_c\|^2}{n} + \sqrt{\frac{3}{2d}} \nu \beta_{bias}(t) + \vartheta_0 \beta_{norm}(t)$ shows Theorem 4.2 when looking at the prediction of the linear model. Recall that [12] showed that the average squared error in predictions between the linear model and the full neural network is $O(\frac{\eta^2 t^2}{d^{2+\Omega(\alpha)}})$. Then by Markov's inequality, we can guarantee that the predictions of the linear model differ by at most $O(\frac{\eta t}{d^{1+\Omega(\alpha)}})$ for at least $1 - O(d^{-\Omega(\alpha)})$ proportion of the examples. This error can be factored into the existing error term. Hence the result holds for the full neural network.

We can apply the same argument for the class c' . Thus Theorem 4.2 is proven.

Notably, Theorem 4.2 only depends on the closeness of the neural network and the initial linear model on the training data, hence does not rely on assumption A.6.

B.3 Proof of Theorem 4.3

Theorem 4.3. *Under the assumptions of Theorem 4.1, if the classes are balanced, and the total size of the minority groups in class c is small, i.e., $O(n^{1-\gamma})$ for some $\gamma > 0$, then there exists a constant $\nu_2 > 0$ such that at $T = \nu_2 \cdot \frac{d \log d}{\eta}$, for an example \mathbf{x}_i in a majority group $g_{c,s}$, the contribution of the core feature to the model's output is at most:*

$$|f(\mathbf{v}_c; \mathbf{W}_T, \mathbf{z}_T)| \leq \sqrt{d} \frac{R_s}{\zeta R_c} + O(n^{-\gamma} \sqrt{d}) + O(d^{-\Omega(\alpha)}). \quad (9)$$

In particular if $\min\{R_c, 1\} \gg R_s$, then the model's output is mostly indicated by the spurious feature instead of the core feature:

$$|f(\mathbf{v}_s; \mathbf{W}_T, \mathbf{z}_T)| \geq \frac{\sqrt{d}}{2\zeta} \gg |f(\mathbf{v}_c; \mathbf{W}_T, \mathbf{z}_T)|. \quad (10)$$

Let g_{maj} be the total number of majority groups among all classes. Note that by the definition of majority groups, g_{maj} is at most the number of classes, namely 2 in the given analysis.

Since the classes are balanced with labels ± 1 , it is not hard to see that the bias term in the weights will always be zero, hence we may as well assume that we do not have the bias term. Abusing notation, we will still denote quantities by the same symbol, even though now the bias term has been removed.

First consider a model $\tilde{f} = \boldsymbol{\psi}^\top \tilde{\boldsymbol{\beta}}$ trained on the dataset \mathcal{D}_{maj} , which only contains examples from the majority groups. Further, assume \mathcal{D}_{maj} has infinitely many examples so that the noise perfectly matches the underlying distribution. We prove the results in this simplified setting then extend the result using matrix perturbations.

We have

$$\begin{aligned} \mathcal{L} &= \frac{1}{2} \mathbb{E}_{\mathcal{D}_{maj}} [(\boldsymbol{\psi}_i^\top \tilde{\boldsymbol{\beta}} - y_i)^2] \\ \nabla \mathcal{L} &= \mathbb{E}_{\mathcal{D}_{maj}} [(\boldsymbol{\psi}_i^\top \tilde{\boldsymbol{\beta}} - y_i) \boldsymbol{\psi}_i] \end{aligned}$$

and the optimal $\tilde{\boldsymbol{\beta}}_*$ satisfies

$$\tilde{\boldsymbol{\beta}}_* = \left(\mathbb{E}_{\mathcal{D}_{maj}} [\boldsymbol{\psi}_i \boldsymbol{\psi}_i^\top] \right)^\dagger \mathbb{E}_{\mathcal{D}_{maj}} [y_i \boldsymbol{\psi}_i]$$

where \dagger represents the Moore-Penrose pseudo-inverse.

Since the noise is symmetrical with respect to the classes, the bias and norm terms of β must be zero. Thus the loss becomes

$$\mathcal{L} = \frac{1}{2} \mathbb{E}_{(\mathbf{x}_i, y_i) \sim \mathcal{D}_{\text{maj}}} \left[\left(\sqrt{\frac{2}{d}} \zeta \mathbf{x}_i^\top \tilde{\beta}' - y_i \right)^2 \right] \quad (21)$$

$$= \frac{1}{2} \mathbb{E}_{\mathcal{D}_{\text{maj}}} \left[\left(\sqrt{\frac{2}{d}} \zeta (\mathbf{v}_{c_i} + \mathbf{v}_{s_i} + \boldsymbol{\xi}_i)^\top \tilde{\beta}' - y_i \right)^2 \right] \quad (22)$$

$$= \frac{1}{2} \mathbb{E}_{\mathcal{D}_{\text{maj}}} \left[\left(\sqrt{\frac{2}{d}} \zeta (\mathbf{v}_{c_i} + \mathbf{v}_{s_i})^\top \tilde{\beta}' - y_i \right)^2 + \left(\sqrt{\frac{2}{d}} \zeta \boldsymbol{\xi}_i^\top \tilde{\beta}' \right)^2 \right] \quad (23)$$

$$= \frac{1}{2} \mathbb{E}_{\mathcal{D}_{\text{maj}}} \left[\left(\sqrt{\frac{2}{d}} \zeta (\mathbf{v}_{c_i} + \mathbf{v}_{s_i})^\top \tilde{\beta}' - y_i \right)^2 \right] + \frac{\zeta^2}{d} \tilde{\beta}'^\top \boldsymbol{\Sigma}_\xi \tilde{\beta}' \quad (24)$$

Consider the model β_s which only learns the spurious features of majority groups

$$\beta'_s = \sqrt{\frac{d}{2}} \frac{1}{\zeta} \sum_{g_{c,s} \text{ is a majority group}} \frac{c \mathbf{v}_s}{\|\mathbf{v}_s\|^2}.$$

Note that for any example in a majority group, $(\mathbf{v}_{c_i} + \mathbf{v}_{s_i})^\top \beta'_s - y_i = 0$. Thus

$$\begin{aligned} \mathcal{L} &= \frac{\zeta^2}{d} \tilde{\beta}'^\top \boldsymbol{\Sigma}_\xi \tilde{\beta}' \\ &= \sum_{\mathbf{v}_s \text{ is spurious}} \frac{\sigma_s^2}{2 \|\mathbf{v}_s\|^2} \\ &\leq \frac{g_{\text{maj}} R^2}{2} \end{aligned}$$

The loss for the optimal model must be smaller. But the loss due to the last term in equation 24 along a core feature alone is

$$\frac{\zeta^2 \sigma_c^2}{\|\mathbf{v}_c\|^2 d} \langle \mathbf{v}_c, \beta'_* \rangle^2 \leq \frac{g_{\text{maj}} R^2}{2}$$

Rearranging gives

$$\langle \mathbf{v}_c, \beta'_* \rangle^2 \leq \frac{d g_{\text{maj}} R^2 \|\mathbf{v}_c\|^2}{2 \zeta^2 \sigma_c^2} \quad (25)$$

Now consider the loss from the first term in equation 24 due to a majority group. It must be at least

$$\begin{aligned} \frac{K}{n} \left(1 - \sqrt{\frac{2}{d}} \zeta \langle \mathbf{v}_s, \beta'_* \rangle - \frac{\sqrt{g_{\text{maj}}} R \|\mathbf{v}_c\|}{\sigma_c} \right)^2 &\leq \frac{g_{\text{maj}} R^2}{2} \\ 1 - \sqrt{\frac{2}{d}} \zeta \langle \mathbf{v}_s, \beta'_* \rangle - \frac{\sqrt{g_{\text{maj}}} R \|\mathbf{v}_c\|}{\sigma_c} &\leq \sqrt{\frac{n g_{\text{maj}} R^2}{2K}} \\ 1 - \sqrt{g_{\text{maj}}} R \left(\frac{\|\mathbf{v}_c\|}{\sigma_c} + \sqrt{\frac{n}{2K}} \right) &\leq \sqrt{\frac{2}{d}} \zeta \langle \mathbf{v}_s, \beta'_* \rangle \end{aligned}$$

Note that $\sqrt{\frac{n}{2K}} \leq \sqrt{\frac{g_{\text{maj}}}{2}}$. Now if we have R sufficiently smaller than $\frac{\sigma_c}{\sqrt{g_{\text{maj}}} \|\mathbf{v}_c\|}$ and $\frac{2}{g_{\text{maj}}}$, we can guarantee that the RHS is at least some constant less than 1, say $\frac{1}{\sqrt{2}}$. In this case, we have

$$\langle \mathbf{v}_s, \beta'_* \rangle^2 \geq \frac{d}{4 \zeta^2} \quad (26)$$

Under these assumptions it is clear from equation 25 that we will also have

$$\frac{d}{4\zeta^2} \gg \langle \mathbf{v}_c, \boldsymbol{\beta}_* \rangle^2 \quad (27)$$

Now we return to the original dataset, which contains minority groups and only a finite number of examples. Again, we have

$$\boldsymbol{\beta}_* = (\boldsymbol{\Psi}^\top \boldsymbol{\Psi})^\dagger \boldsymbol{\Psi}^\top \mathbf{y}$$

Since we have removed the bias term, it is not hard to show that the matrix $\frac{1}{n} \boldsymbol{\Psi}^\top \boldsymbol{\Psi}$ has all eigenvalues of order $\Theta(\frac{1}{d})$. Now consider the difference between $\|\frac{1}{n} \boldsymbol{\Psi}^\top \boldsymbol{\Psi}\|$ and $\|\mathbb{E}_{\mathcal{D}_{\text{maj}}}[\boldsymbol{\psi}_i \boldsymbol{\psi}_i^\top]\|$. With high probability it will be of order $O(\frac{n_{\text{mino}}}{nd} + \frac{1}{d\sqrt{n}}) = O(\frac{n^{-\gamma}}{d})$, where the first term corresponds to the inclusion of minority groups and the second term corresponds having a finite sample size. It follows that

$$\begin{aligned} \left\| \left(\frac{1}{n} \boldsymbol{\Psi}^\top \boldsymbol{\Psi} \right)^\dagger - \left(\mathbb{E}_{\mathcal{D}_{\text{maj}}}[\boldsymbol{\psi}_i \boldsymbol{\psi}_i^\top] \right)^\dagger \right\| &= O\left(d - \frac{d}{d - O(n^{-\gamma})}\right) \\ &= O(dn^{-\gamma}) \end{aligned}$$

A similar argument shows that

$$\|\boldsymbol{\Psi}^\top \mathbf{y} - \mathbb{E}_{\mathcal{D}_{\text{maj}}}[\mathbf{y}_i \boldsymbol{\psi}_i]\| = O(d^{-\frac{1}{2}} n^{-\gamma})$$

Thus the change in alignment with a feature \mathbf{v} is

$$\begin{aligned} \left\| \langle \tilde{\boldsymbol{\beta}}_*, \mathbf{v} \rangle - \langle \boldsymbol{\beta}_*, \mathbf{v} \rangle \right\| &= \left\| (\boldsymbol{\Psi}^\top \boldsymbol{\Psi})^\dagger \boldsymbol{\Psi}^\top \mathbf{y} - \left(\mathbb{E}_{\mathcal{D}_{\text{maj}}}[\boldsymbol{\psi}_i \boldsymbol{\psi}_i^\top] \right)^\dagger \mathbb{E}_{\mathcal{D}_{\text{maj}}}[\mathbf{y}_i \boldsymbol{\psi}_i] \right\| \|\mathbf{v}\| \\ &\leq \left\| \left((\boldsymbol{\Psi}^\top \boldsymbol{\Psi})^\dagger - \left(\mathbb{E}_{\mathcal{D}_{\text{maj}}}[\boldsymbol{\psi}_i \boldsymbol{\psi}_i^\top] \right)^\dagger \right) \boldsymbol{\Psi}^\top \mathbf{y} \right. \\ &\quad \left. + \left(\mathbb{E}_{\mathcal{D}_{\text{maj}}}[\boldsymbol{\psi}_i \boldsymbol{\psi}_i^\top] \right)^\dagger (\boldsymbol{\Psi}^\top \mathbf{y} - \mathbb{E}_{\mathcal{D}_{\text{maj}}}[\mathbf{y}_i \boldsymbol{\psi}_i]) \right\| \|\mathbf{v}\| \\ &\leq O\left((dn^{-\gamma})(d^{-\frac{1}{2}}) + d(d^{-\frac{1}{2}} n^{-\gamma})\right) \\ &\leq O(n^{-\gamma} \sqrt{d}) \end{aligned}$$

Replacing g_{maj} with 2, and combining equations 25, 26 28, and ASumption A.6, we get

$$|f(\mathbf{v}_s; \mathbf{W}_T, \mathbf{z}_T)| \geq \frac{\sqrt{d}}{2\zeta} \gg \sqrt{d} \frac{R_s}{\zeta R_c} + \mathcal{O}(n^{-\gamma} \sqrt{d}) + \mathcal{O}(d^{-\Omega(\alpha)}) \geq |f(\mathbf{v}_c; \mathbf{W}_T, \mathbf{z}_T)|. \quad (28)$$

which proves the theorem.

C Experimentation Details

C.1 Datasets

CMNIST We created a colored MNIST dataset with spurious correlations by using colors as spurious attributes following the settings in [41]. First, we defined an image classification task with 5 classes by grouping consecutive digits (0 and 1, 2 and 3, 4 and 5, 6 and 7, 8 and 9) into the same class. From the train split, we randomly selected 50,000 examples as the training set, while the remaining 10,000 samples were used as the validation set. The test split follows the official test split of MNIST.

For each class y_i , we assigned a color \mathbf{v}_s from a set of colors $\mathcal{A} = \{\text{\#ff0000}, \text{\#85ff00}, \text{\#00fff3}, \text{\#6e00ff}, \text{\#ff0018}\}$ as the spurious attribute that highly correlates with this class, represented by their hex codes, to the foreground of a fraction p_{corr} of the training examples. This fraction represents the majority group for class y_i . The stronger the spurious correlation between class y_i and the spurious attribute \mathbf{v}_s , the higher the value of p_{corr} . The remaining $1 - p_{\text{corr}}$ training examples were randomly colored using a color selected from $\mathcal{A} \setminus \mathbf{v}_s$. In our experiments, we set $p_{\text{corr}} = 0.995$ to establish significant spurious correlations within the dataset.

Waterbirds is introduced by [28] to study the spurious correlation between the background (land/water) and the foreground (landbird/waterbird) in image recognition. Species in Caltech-UCSD Birds-200-2011 (CUB-200-2011) dataset [38] are grouped into two classes, waterbirds and landbirds. All birds are then cut and pasted onto new background images, with waterbirds more likely to appear on water and landbirds having a higher probability on land. There are 4795 training examples in total, 3498 for landbirds with land background, 184 for landbirds with water background, 56 for waterbirds with land background, and 1057 for waterbirds with water background.

CelebA is a large-scale face attribute dataset comprised of photos of celebrities. Each image is annotated with 40 binary attributes, in which “blond hair” and “male” are commonly used for studying spurious correlations. Specifically, gender is considered a spurious feature for hair color classification. The smallest group is blond male.

C.2 Hyperparameters

The hyperparameters employed in our experiments on spurious benchmarks are detailed in Table 5. For the Waterbirds and CelebA datasets, we tuned the learning rate within the range of $\{1e-4, 1e-5\}$ and weight decay within the range of $\{1e-1, 1e-0\}$. These ranges were determined based on the ranges of optimal hyperparameters used by the current state-of-the-art algorithms [6, 16, 28, 23, 41]. The batch sizes and total training epochs remained consistent with those used in these prior studies. To determine the epoch for separating groups, we performed clustering on the validation set while training the model on the training set to maximize the minimum recall of SPARE’s clusters with the groups in the validation set. As mentioned in Section 6.2, we decided the number of clusters and adjusted the sampling power for each class based on Silhouette scores. Specifically, when the Silhouette score was below 0.9, a sampling power of 2 was applied, while a sampling power of 1 was used otherwise. It is important to note that other algorithms tuned hyperparameters, such as epochs to separate groups and upweighting factors, by maximizing the worst-group accuracy of fully trained models on the validation set, which is more computationally demanding than the hyperparameter tuning of SPARE.

Table 5: Hyperparameters used for the reported results on different datasets.

DATASET	CMNIST	WATERBIRDS	CELEBA
LEARNING RATE	1E-3	1E-4	1E-5
WEIGHT DECAY	1E-3	1E-1	1E-0
BATCH SIZE	32	128	128
TRAINING EPOCHS	20	300	50
GROUP SEPARATION EPOCH	2	2	1
SILHOUETTE SCORES	[0.997,0.978,0.996,0.991,0.996]	[0.886,0.758]	[0.924,0.757]
SAMPLING POWER	[1,1,1,1,1]	[2,2]	[1,2]

C.3 Choices of Model Outputs

In our experiments, we found the worst-group accuracy gets the most improvement when SPARE uses the outputs of the last linear layer to separate the majority from the minority for CMNIST and Waterbirds and use the second to last layer (i.e., the feature embeddings inputted to the last linear layer) to identify groups in CelebA. We speculate that this phenomenon can be attributed to the increased complexity of the CelebA dataset compared to the other two datasets, as employing a higher output dimension help identify groups more effectively.

D Discovering Spurious Features

D.1 Restricted ImageNet

We use Restricted ImageNet proposed in [37] which contains 9 superclasses of ImageNet. The classes and the corresponding ImageNet class ranges are shown in Table 6.

Table 6: Classes included in Restricted ImageNet and their corresponding ImageNet class ranges.

Restricted ImageNet Class	ImageNet class range
dog	151-268
cat	281-285
frog	30-32
turtle	33-37
bird	80-100
primate	365-382
fish	389-397
crab	118-121
insect	300-319

D.2 Experimental Settings

When training on Restricted ImageNet, we use ResNet50 [10] from the PyTorch library [25] with randomly initialized weights instead of pretrained weights. We followed the hyperparameters specified in [8]: the model was trained for 90 epochs, with an initial learning rate of 0.1. The learning rate was reduced by a factor of 0.1 at the 30th, 60th, and 80th epochs. During training, we employed Nesterov momentum of 0.9 and applied a weight decay of 0.0001.

D.3 Investigation on Groups Identified by EIIL vs. SPARE

Evaluation setup. As no group-labeled validation set is available to tune the epoch in which the groups are separated, we tried separating groups using ERM models trained for various numbers of epochs. Since both EIIL and SPARE identify the groups early (EIIL infers groups on models trained with ERM for 1 epoch for both Waterbirds and CelebA, as shown in Table 10 and Table 9, and 5 epochs for CMNIST; the group separation epochs for SPARE are epoch 1 or 2 for the three datasets, as shown in Table 5), we tuned the epoch to separate groups in the range of {2,4,6,8} for both algorithms. This tuning was based on the average test accuracy achieved by the final model, as the worst-group accuracy is undefined without group labels. Interestingly, while SPARE did not show sensitivity to the initial epochs on Restricted ImageNet, EIIL achieved the highest average test accuracy when the initial models were trained for 4 epochs using ERM.

EIIL finds groups of misclassified examples while SPARE finds groups with spurious features. We observed that EIIL effectively separates examples that have 0% classification accuracy as the minority group, as demonstrated in Table 7. This separation is analogous to the error-splitting strategy employed by JTT [16] when applied to the same initial model. This similarity in behavior is also discussed in [6]. Instead of focusing on misclassified examples, SPARE separates the examples that are learned early in training. Table 8 shows that the first cluster found by SPARE have almost 100% accuracy, indicating that the spurious feature is learned for such examples. Downweighting examples that are learned early allows for effectively mitigating the spurious correlation.

SPARE upweights outliers less than EIIL. Heavily upweighting misclassified examples can be problematic for this more realistic dataset than the spurious benchmarks as the misclassified ones are likely to be outliers, noisy-labeled or contain non-generalizable information. Table 7 shows that groups inferred by EIIL are more imbalanced, which makes EIIL upweights misclassified examples more than SPARE. As shown in Table 4, this heavier upweighting of misclassified examples with EIIL drops accuracy not only for the minority groups but also for the overall accuracy. Therefore, we anticipate that this effect would persist or become even more pronounced for methods like JTT, which directly identify misclassified examples as the minority group. In contrast, SPARE separates groups based on the spurious feature that is learned early, and upweights the misclassified examples less than other methods due to the more balanced size of the clusters. This allows SPARE to more effectively mitigate spurious correlations than others.

Table 7: Accuracy (%) of training examples in different classes of Restricted ImageNet in the two environments inferred by EIIL. EIIL trains models with Group DRO on the inferred environments, resulting in up-weighting misclassified examples in Env 2.

Class	dog	cat	frog	turtle	bird	primate	fish	crab	insect
Env 1 ERM acc	98	37	26	62	76	78	78	71	90
Env 2 ERM acc	0	0	0	0	0	0	0	0	0
Env 1 size	144378	488	457	2875	17157	11233	6817	2172	21112
Env 2 size	3495	6012	3443	3625	9984	12167	4417	3028	4888

Table 8: Accuracy (%) of training examples in different classes of Restricted ImageNet in the two groups inferred by SPARE at epoch 8.

Class	dog	cat	frog	turtle	bird	primate	fish	crab	insect
Cluster 1 ERM acc	100	100	100	100	100	99	100	100	100
Cluster 2 ERM acc	64	9	11	14	28	13	27	16	36
Cluster 1 size	130541	3236	1578	2684	18870	12158	7331	2566	18974
Cluster 2 size	17332	3264	2322	3816	8271	11242	3903	2634	7026

E Comparing Inferred with Ground-truth Groups

In Table 9 and Table 10, we compare the clusters found by SPARE vs. (1) misclassified examples found by JTT, (2) environments inferred by EIIL, and (3) pseudo-labels learned by SSA.

E.1 Implementation of Baselines

Both JTT [16] and EIIL [6] require training an ERM model to identify groups of examples for upweighting or downweighting. For clarity, we will refer to this ERM model as the *reference model*, which is equivalent to the *identification models* defined in [16].

JTT. We train the reference model from ImageNet-pre-trained weights with ERM based on the optimal hyperparameters reported in [16] and upsample training examples misclassified by the identification models. For Waterbirds, we train the identification model for 60 epochs with a learning rate $1e-5$ and weight decay 1. For CelebA, the identification model is trained for 1 epoch with a learning rate $1e-5$ and weight decay 0.1.

EIIL. For Waterbirds, we follow the environment inference steps explained in [6]: we use an ERM model trained for 1 epoch as the reference model and optimize the EI objective of EIIL with learning rate 0.01 for 20, 000 steps using the Adam optimizer. As no experiment was conducted on CelebA in the original paper [6], we follow the proposal in [23], which took the same EI procedure for CelebA as for Waterbirds.

SSA. We implement SSA based on the pseudo-code and experimental details explained in [23]. Please refer to [23] for details of the setups. As the pseudo-attribute predictor shares the same architecture as the robust model but is trained on the validation set, to make the inference cost comparable across all methods, we report the inference cost of SSA by converting the number of training-on-validation steps for the pseudo-attribute predictor to the number of training-on-train epochs that involve the same total number of gradient backward steps.

E.2 Comparison of Groups.

CelebA. We start from the CelebA dataset, where we observed more significant disparities among the groups identified by different algorithms, as demonstrated in Table 9. JTT simply upweights the smaller class (i.e., blond hair), as most examples from that class are misclassified due to the strong class imbalance. Similarly, EIIL assigns higher weights to more examples from the smaller class.

On the other hand, when examining the confusion matrices, we found that both SSA and SPARE successfully discover groups that closely align with the ground-truth groups in CelebA. Note that SPARE requires much less training than SSA. However, upon visualizing the samples, we noticed that the upweighted examples identified by SSA exhibit some characteristics learned from the validation set that are more correlated with a certain gender. For instance, 11.4% of the upweighted examples of blonde females and only 1.2% of the downweighted examples wear sunglasses, which is a feature that is correlated more with males in the validation set (13.5% of males vs. only 2.3% of females in the validation set wear sunglasses). Importantly, when examining the correlation between hair colors (actual class labels) and sunglasses, we observe a milder correlation between non-blond hair and sunglasses: 7.3% of non-blond haired wear sunglasses compared to only 1.7% of those with blond hair. Therefore, the pseudo-attribute predictor has likely learned to correlate blond males with sunglasses, resulting in the potential to amplify other (potentially spurious) correlations learned from the validation set while mitigating the targeted spurious correlations.

Waterbirds. In line with our observations on CelebA, as shown in Table 10, the groups identified by JTT are similar to those identified by EIL, and the groups identified by SSA share similarities with the groups identified by SPARE, which requires less training. Specifically, JTT and EIL focus on upweighting noisy and outlier examples, SSA upweights examples that may possess certain (spurious) features (i.e., yellow feathers), and SPARE prioritizes upweighting minority groups that do not share the spurious features with the majority groups.

F Reproducibility

Each experiment was conducted on one of the following GPUs: NVIDIA A40 with 45G memory, NVIDIA RTX A6000 with 48G memory, and NVIDIA RTX A5000 with 24G memory.

Table 9: Comparison of groups found by different methods for CelebA.



















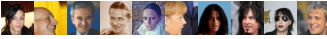
















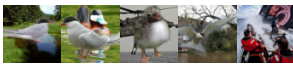
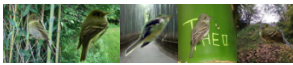


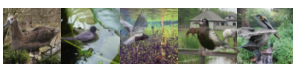

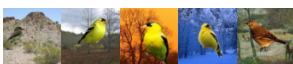

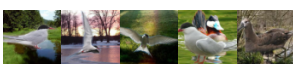

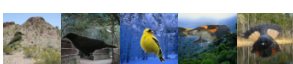

Inference (Cost)	Method	Samples	Confusion Matrix																															
JTT (1 epoch)	dark-female upweight		<table><tr><td rowspan="4">True groups</td><td>Dark female</td><td>3</td><td>71626</td><td>0</td><td>0</td></tr><tr><td>Dark male</td><td>0</td><td>66874</td><td>0</td><td>0</td></tr><tr><td>Blonde female</td><td>0</td><td>0</td><td>170</td><td>22710</td></tr><tr><td>Blonde male</td><td>0</td><td>0</td><td>0</td><td>1387</td></tr><tr><td></td><td>Dark upsample</td><td>Dark downsample</td><td>Blonde downsample</td><td>Blonde upsample</td></tr><tr><td colspan="5">Predicted groups</td></tr></table>	True groups	Dark female	3	71626	0	0	Dark male	0	66874	0	0	Blonde female	0	0	170	22710	Blonde male	0	0	0	1387		Dark upsample	Dark downsample	Blonde downsample	Blonde upsample	Predicted groups				
	True groups	Dark female			3	71626	0	0																										
		Dark male			0	66874	0	0																										
		Blonde female			0	0	170	22710																										
		Blonde male		0	0	0	1387																											
		Dark upsample		Dark downsample	Blonde downsample	Blonde upsample																												
	Predicted groups																																	
	dark-female downweight																																	
dark-male upweight																																		
dark-male downweight																																		
blonde-female downweight																																		
blonde-female upweight																																		
blonde-male downweight																																		
blonde-male upweight																																		
EIL (1 epoch)	dark-female upweight		<table><tr><td rowspan="4">True groups</td><td>Dark female</td><td>3128</td><td>68501</td><td>0</td><td>0</td></tr><tr><td>Dark male</td><td>331</td><td>66543</td><td>0</td><td>0</td></tr><tr><td>Blonde female</td><td>0</td><td>0</td><td>4404</td><td>18476</td></tr><tr><td>Blonde male</td><td>0</td><td>0</td><td>1028</td><td>359</td></tr><tr><td></td><td>Dark upsample</td><td>Dark downsample</td><td>Blonde downsample</td><td>Blonde upsample</td></tr><tr><td colspan="5">Predicted groups</td></tr></table>	True groups	Dark female	3128	68501	0	0	Dark male	331	66543	0	0	Blonde female	0	0	4404	18476	Blonde male	0	0	1028	359		Dark upsample	Dark downsample	Blonde downsample	Blonde upsample	Predicted groups				
	True groups	Dark female			3128	68501	0	0																										
		Dark male			331	66543	0	0																										
		Blonde female			0	0	4404	18476																										
		Blonde male		0	0	1028	359																											
		Dark upsample		Dark downsample	Blonde downsample	Blonde upsample																												
	Predicted groups																																	
	dark-female downweight																																	
dark-male upweight																																		
dark-male downweight																																		
blonde-female downweight																																		
blonde-female upweight																																		
blonde-male downweight																																		
blonde-male upweight																																		
SSA (53 epochs)	dark-female upweight		<table><tr><td rowspan="4">True groups</td><td>Dark female</td><td>68642</td><td>2987</td><td>0</td><td>0</td></tr><tr><td>Dark male</td><td>2105</td><td>64769</td><td>0</td><td>0</td></tr><tr><td>Blonde female</td><td>0</td><td>0</td><td>22547</td><td>333</td></tr><tr><td>Blonde male</td><td>0</td><td>0</td><td>102</td><td>1285</td></tr><tr><td></td><td>Dark upsample</td><td>Dark downsample</td><td>Blonde downsample</td><td>Blonde upsample</td></tr><tr><td colspan="5">Predicted groups</td></tr></table>	True groups	Dark female	68642	2987	0	0	Dark male	2105	64769	0	0	Blonde female	0	0	22547	333	Blonde male	0	0	102	1285		Dark upsample	Dark downsample	Blonde downsample	Blonde upsample	Predicted groups				
	True groups	Dark female			68642	2987	0	0																										
		Dark male			2105	64769	0	0																										
		Blonde female			0	0	22547	333																										
		Blonde male		0	0	102	1285																											
		Dark upsample		Dark downsample	Blonde downsample	Blonde upsample																												
	Predicted groups																																	
	dark-female downweight																																	
dark-male upweight																																		
dark-male downweight																																		
blonde-female downweight																																		
blonde-female upweight																																		
blonde-male downweight																																		
blonde-male upweight																																		
SPARE (1 epoch)	dark-female upweight		<table><tr><td rowspan="4">True groups</td><td>Dark female</td><td>61568</td><td>10061</td><td>0</td><td>0</td></tr><tr><td>Dark male</td><td>5440</td><td>61434</td><td>0</td><td>0</td></tr><tr><td>Blonde female</td><td>0</td><td>0</td><td>21135</td><td>1745</td></tr><tr><td>Blonde male</td><td>0</td><td>0</td><td>257</td><td>1130</td></tr><tr><td></td><td>Dark upsample</td><td>Dark downsample</td><td>Blonde downsample</td><td>Blonde upsample</td></tr><tr><td colspan="5">Predicted groups</td></tr></table>	True groups	Dark female	61568	10061	0	0	Dark male	5440	61434	0	0	Blonde female	0	0	21135	1745	Blonde male	0	0	257	1130		Dark upsample	Dark downsample	Blonde downsample	Blonde upsample	Predicted groups				
	True groups	Dark female			61568	10061	0	0																										
		Dark male			5440	61434	0	0																										
		Blonde female			0	0	21135	1745																										
		Blonde male		0	0	257	1130																											
		Dark upsample		Dark downsample	Blonde downsample	Blonde upsample																												
	Predicted groups																																	
	dark-female downweight																																	
dark-male upweight																																		
dark-male downweight																																		
blonde-female downweight																																		
blonde-female upweight																																		
blonde-male downweight																																		
blonde-male upweight																																		

Table 10: Comparison of groups found by different methods for Waterbirds.

Inference (Cost)	Method	Samples	Confusion Matrix																												
JTT (60 epochs)	landbird-land downweight		<table><tr><td>Landbird land</td><td>3489</td><td>9</td><td>0</td><td>0</td></tr><tr><td>Landbird water</td><td>114</td><td>70</td><td>0</td><td>0</td></tr><tr><td>Waterbird land</td><td>0</td><td>0</td><td>51</td><td>5</td></tr><tr><td>Waterbird water</td><td>0</td><td>0</td><td>171</td><td>886</td></tr><tr><td>Landbird downweight</td><td>Landbird upweight</td><td>Waterbird upweight</td><td>Waterbird downweight</td></tr><tr><td colspan="4">Predicted groups</td></tr></table>	Landbird land	3489	9	0	0	Landbird water	114	70	0	0	Waterbird land	0	0	51	5	Waterbird water	0	0	171	886	Landbird downweight	Landbird upweight	Waterbird upweight	Waterbird downweight	Predicted groups			
	Landbird land	3489		9	0	0																									
	Landbird water	114		70	0	0																									
	Waterbird land	0		0	51	5																									
	Waterbird water	0		0	171	886																									
Landbird downweight	Landbird upweight	Waterbird upweight	Waterbird downweight																												
Predicted groups																															
landbird-land upweight																															
waterbird-water downweight																															
waterbird-water upweight																															
EIL (1 epoch)	landbird-land downweight		<table><tr><td>Landbird land</td><td>3477</td><td>21</td><td>0</td><td>0</td></tr><tr><td>Landbird water</td><td>86</td><td>98</td><td>0</td><td>0</td></tr><tr><td>Waterbird land</td><td>0</td><td>0</td><td>41</td><td>15</td></tr><tr><td>Waterbird water</td><td>0</td><td>0</td><td>74</td><td>983</td></tr><tr><td>Landbird downweight</td><td>Landbird upweight</td><td>Waterbird upweight</td><td>Waterbird downweight</td></tr><tr><td colspan="4">Predicted groups</td></tr></table>	Landbird land	3477	21	0	0	Landbird water	86	98	0	0	Waterbird land	0	0	41	15	Waterbird water	0	0	74	983	Landbird downweight	Landbird upweight	Waterbird upweight	Waterbird downweight	Predicted groups			
	Landbird land	3477		21	0	0																									
	Landbird water	86		98	0	0																									
	Waterbird land	0		0	41	15																									
	Waterbird water	0		0	74	983																									
Landbird downweight	Landbird upweight	Waterbird upweight	Waterbird downweight																												
Predicted groups																															
landbird-land upweight																															
waterbird-water downweight																															
waterbird-water upweight																															
SSA (40 epochs)	landbird-land downweight		<table><tr><td>Landbird land</td><td>3301</td><td>197</td><td>0</td><td>0</td></tr><tr><td>Landbird water</td><td>11</td><td>173</td><td>0</td><td>0</td></tr><tr><td>Waterbird land</td><td>0</td><td>0</td><td>53</td><td>3</td></tr><tr><td>Waterbird water</td><td>0</td><td>0</td><td>83</td><td>974</td></tr><tr><td>Landbird downweight</td><td>Landbird upweight</td><td>Waterbird upweight</td><td>Waterbird downweight</td></tr><tr><td colspan="4">Predicted groups</td></tr></table>	Landbird land	3301	197	0	0	Landbird water	11	173	0	0	Waterbird land	0	0	53	3	Waterbird water	0	0	83	974	Landbird downweight	Landbird upweight	Waterbird upweight	Waterbird downweight	Predicted groups			
	Landbird land	3301		197	0	0																									
	Landbird water	11		173	0	0																									
	Waterbird land	0		0	53	3																									
	Waterbird water	0		0	83	974																									
Landbird downweight	Landbird upweight	Waterbird upweight	Waterbird downweight																												
Predicted groups																															
landbird-land upweight																															
waterbird-water downweight																															
waterbird-water upweight																															
SPARE (1 epoch)	landbird-land downweight		<table><tr><td>Landbird land</td><td>3431</td><td>67</td><td>0</td><td>0</td></tr><tr><td>Landbird water</td><td>45</td><td>139</td><td>0</td><td>0</td></tr><tr><td>Waterbird land</td><td>0</td><td>0</td><td>50</td><td>6</td></tr><tr><td>Waterbird water</td><td>0</td><td>0</td><td>126</td><td>931</td></tr><tr><td>Landbird downweight</td><td>Landbird upweight</td><td>Waterbird upweight</td><td>Waterbird downweight</td></tr><tr><td colspan="4">Predicted groups</td></tr></table>	Landbird land	3431	67	0	0	Landbird water	45	139	0	0	Waterbird land	0	0	50	6	Waterbird water	0	0	126	931	Landbird downweight	Landbird upweight	Waterbird upweight	Waterbird downweight	Predicted groups			
	Landbird land	3431		67	0	0																									
	Landbird water	45		139	0	0																									
	Waterbird land	0		0	50	6																									
	Waterbird water	0		0	126	931																									
Landbird downweight	Landbird upweight	Waterbird upweight	Waterbird downweight																												
Predicted groups																															
landbird-land upweight																															
waterbird-water downweight																															
waterbird-water upweight	